Biasing HER4 tyrosine kinase signaling with antibodies: Induction of cell death by antibody-dependent HER4 intracellular domain trafficking

Romain Lanotte, Véronique Garambois, Nadège Gaborit, Christel Larbouret, Astrid Musnier, Pierre Martineau, André Pèlegrin, Thierry Chardès

Biasing HER4 tyrosine kinase signaling with antibodies: Induction of cell death by antibody-dependent HER4 intracellular domain trafficking

Romain Lanotte, Véronique Garambois, Nadège Gaborit, Christel Larbouret, Astrid Musnier, Pierre Martineau, André Pèlegrin, Thierry Chardès

Biasing HER4 Tyrosine Kinase Signaling with Antibodies: Induction of Cell Death by Antibody-Dependent HER4 intracellular domain Trafficking

Romain Lanotte[1], Véronique Garambois[1], Nadège Gaborit[1,4], Christel Larbouret[1], Astrid Musnier[2], Pierre Martineau[1], André Pèlegrin[1], and Thierry Chardès[1,3]

[1]Institut de Recherche en Cancérologie de Montpellier (IRCM), INSERM U1194, Université de Montpellier, Institut régional du Cancer de Montpellier (ICM), Montpellier, 34298, France

[2]MAbSilico SAS, Centre de Recherche INRA Val de Loire, Nouzilly, 37380, France

[3]Centre National de la Recherche Scientifique (CNRS)

Present Address

[4]Institut de Génétique Humaine, CNRS UMR 9002, 141 rue de la Cardonille, 34396, Montpellier cedex 5, France

Corresponding author

Dr Thierry Chardès

Institut de Recherche en Cancérologie de Montpellier, Montpellier, 34298, France

thierry.chardes@inserm.fr

Phone number: (33) 467 612 404

Fax number: (33) 467 613 727

Keywords

HER4, 4ICD, neuregulin, antibody, cancer

Word count: 5720

Number of Figures: 7

Number of Tables: 0

Number of Supporting Informations: 1

Number of Supporting Figures: 6

Number of Supporting Tables: 1

Abstract

HER4 isoforms have oncogenic or tumor suppressor functions depending on their susceptibility to proteolytic cleavage and HER4 Intracellular Domain (4ICD) translocation. Here, we report that the NRG1 tumor suppressor mechanism through the HER4 JMa/CYT1 isoform can be mimicked by the agonist anti-HER4 antibody C6. NRG1 induced cleavage of poly(ADP-ribose) polymerase (PARP) and sub-G1 DNA fragmentation, and also reduced the metabolic activity of HER3-negative/HER4-positive cervical (C-33A) and ovarian (COV318) cancer cells. This effect was confirmed in HER4 JMa/CYT1-, but not JMa/CYT2-transfected BT549 triple-negative breast cancer cells. NRG1 favored 4ICD cleavage and retention in mitochondria in JMa/CYT1-transfected BT549 cells, leading to Reactive Oxygen Species (ROS) production through mitochondrial depolarization. Similarly, the anti-HER4 antibody C6, which binds to a conformational epitope located on aa 575-592 and 605-620 of HER4 domain IV, induced 4ICD cleavage and retention in mitochondria, and mimicked NRG1-mediated effects on PARP cleavage, ROS production, and mitochondrial membrane depolarization in cancer cells. *In vivo*, C6 reduced growth of COV434 and HCC1187 tumor cell xenografts in nude mice. Biasing 4ICD trafficking to mitochondria with anti-HER4 antibodies to mimic NRG1 suppressor functions could be an alternative anti-cancer strategy.

Abbreviations:

4ICD, HER4 intracellular domain; ROS, Reactive Oxygen Species; poly(ADP-ribose) polymerase, PARP; NRG1, neuregulin 1; RTK, Receptor Tyrosine Kinase;

1. INTRODUCTION

The Human Epidermal growth factor Receptor's family (HER or ErbB) includes four Receptor Tyrosine Kinases (RTK; EGFR/HER1, HER2, HER3 and HER4) that play roles in development and cancer. EGFR and HER2 role in cancer progression led to the development of monoclonal antibodies (mAbs) against these receptors, such as cetuximab and trastuzumab [1]. More recently, HER3 also has been considered a key player in tumor signaling and resistance to cancer drugs, leading to the development of anti-HER3 mAbs [2]. Conversely, results with antagonist mAbs against HER4 have been disappointing, and currently no anti-HER4 mAb is used in the clinic.

HER4 is unusual among HER members. Its biology is more complex and its role in cancer is still controversial. HER4 is expressed in various cancers, such as blastoma, breast, lung, melanoma, pancreas, gastric, colorectal, ovarian and bladder cancer [3]. However, the prognostic significance of HER4 expression in cancer remains unclear, particularly in breast cancer where HER4 has been alternatively described as an oncogene [4] and a tumor suppressor [5]. These opposite effects are explained by the existence of four HER4 isoforms at the cell surface, each with its own downstream signaling pathway [6]. These isoforms (JMa/CYT1, JMa/CYT2, JMb/CYT1 and JMb/CYT2) differ in their ExtraCellular Domain (ECD) and IntraCellular Domain (ICD). Following activation, JMa isoforms are cleaved by a two-step process, catalyzed by TACE and then γ-secretase and called Regulated Intramembrane Proteolysis (RIP), to release the HER4 ECD and ICD (4ICD) [7]. 4ICD translocates to the nucleus where it acts on gene transcription to control multiple cellular pathways (differentiation, migration, proliferation) [8]. Conversely, JMb isoforms are not cleaved and act as classical RTKs. HER4 isoforms acquire the cytoplasmic domain CYT1 or CYT2 by alternative splicing [9]. CYT2 isoforms can only induce phosphorylation of MAPK pathway components, whereas the 16-amino acid extension present only in CYT1 isoforms allows the activation of the MAPK and also of the PI3K pathway [10].

Most studies describe HER4 isoforms and their main ligand NRG1 as oncogenes. JMa/CYT1 and JMa/CYT2 are widely co-expressed. Conversely, expression of JMb variants seems to be restricted to some tissues [6]. In cancer, JMa/CYT1 and JMa/CYT2 have been associated with poor prognosis, due to 4ICD translocation to the nucleus [11]. JMa/CYT1 has been implicated in tumor progression [12], and JMa/CYT2 is considered the most oncogenic isoform. Indeed, CYT2 is more stable than CYT1 in the cytosol [13], and its nuclear location is more robust, with better transcriptional activity [14]. Moreover, CYT2 can activate hyperplasia-related pathways, such as Wnt, β-catenin, and KITENIN [15], and JMa/CYT2 homodimers are constitutively phosphorylated to promote ligand-independent growth [16]. Both isoforms support cancer cell proliferation by modulating numerous signaling pathways [17].

However, in breast cancer, CYT1 isoforms have been associated also with inhibition of cancer cell proliferation [18]. In the cytosol of breast cancer cells, 4ICD directly induces apoptosis from mitochondria through its BH3-only domain [19], explaining the better survival of patients with high cytosolic 4ICD expression [20]. As HER4 plays a role in tissue homeostasis [21], which requires regulation of proliferation and cell death [22], HER4 and 4ICD might also play a tumor suppressor function that could be modulated by NRG1. Indeed, the *ERBB4* promoter is hypermethylated in cancer, and HER4 re-expression using demethylating agents induces apoptosis of breast cancer cells after NRG1 stimulation [23]. In breast cancer, NRG1 and HER4 induce cell cycle arrest by activating JNK through BRCA1 [24], and 4ICD might be a mitotic checkpoint [25], regulating cell cycle progression.

As NRG1 is considered a potential tumor suppressor gene [26] and the Y1056 residue in HER4-CYT1 variants is essential for tumor suppression [27], we hypothesized that the HER4 JMa/CYT1-NRG1 axis has a tumor suppressor function by localizing 4ICD in mitochondria where it can induce apoptosis through its BH3-only domain [19]. We also hypothesized that this NRG1-4ICD pathway could be activated by biased agonist or positive allosteric modulator mAbs, as described for G-Protein Coupled Receptor (GPCR) targeting [28]. By inducing specific

conformational changes in the targeted receptor, these mAbs can selectively modulate specific signaling pathways [29]. Here, we demonstrated that NRG1 induces HER4 JMa/CYT1-expressing cancer cell death through 4ICD retention in mitochondria, and that the anti-HER4 antibody C6 mimics these NRG1-induced effects, leading to growth inhibition of ovarian and breast cancer xenografts.

2. MATERIALS AND METHODS

2.1. Cell cultures

C-33A cervical cancer, COV318 and COV434 ovarian cancer, BT549 and HCC1187 triple-negative breast cancer (TNBC) cells, HEK293T and NIH3T3 cells were obtained from American Type Culture Collection (ATCC) (Rockville, MD), and cultured as described in Supporting Informations 1.

2.2. Recombinant Proteins and Constructs

All recombinant proteins and constructs are indicated in Supporting Informations 1 and Table S1.

2.3. Phage display selection and production of full-length IgGs

Two phage display selection experiments were performed in parallel: the first using NRG1-stimulated JMa/CYT1-transfected cells (whole cell panning by phage display) and the second using recombinant human HER4 ECD as targets. For the first one, JMa/CYT1-transfected NIH3T3 cells were stimulated with 50 ng/ml NRG1 at 37°C for 15min (to activate HER4) and then incubated with the HUSCI proprietary scFv library [30]. After incubation, cells were washed twenty times with PBS and phages were eluted with TPCK trypsin (Thermo Fisher) at room temperature for 10min. Eluted phages were amplified in TG1 bacteria (Agilent, Santa Clara, CA), rescued with the KM13 helper phage (New England Biolabs, Omaha, NE), and used for two other rounds of selection. Screening of eluted phages from the third round were both performed by ELISA and flow cytometry, and selected anti-HER4 scFv were then produced in IgG format, as indicated in Supporting Informations 1.

2.4. HER4 JMa/CYT1- and JMa/CYT2-encoding plasmid transfection in BT549 and C-33A cells

To ensure uniformity of transfection among experimental conditions and experiments, BT549

and C-33A cells were seeded in 150 mm Petri dishes and grown for 24h. Cells were transfected at 70% confluence with 15 μg of JMa/CYT1 or JMa/CYT2 plasmid and 240 μg of PEI diluted in 150mM NaCl solution for 5h. Medium (10% FBS) was then replaced by 1% FBS-medium. Next day, transfected cells were seeded in 6-well or 12-well plates (10% FBS-medium) and grown for 10h. Cells were then starved in 1% FBS-medium for 12h before NRG1 stimulation or antibody treatment.

2.5. Flow cytometry analysis

Cell surface receptor expression was analyzed in all cell lines with the following antibodies: cetuximab (EGFR) (Merck), trastuzumab (HER2) (Roche), SGP1 (HER3) (Santa Cruz Biotechnology), and H4.77.16 (HER4) (Thermo Fisher). Cetuximab and trastuzumab were purchased from the pharmacy of the ICM hospital. Exponentially growing cells were harvested and resuspended in FACS buffer (PBS/1% FBS). $3x10^5$ cells were incubated with 10 μg/ml of primary antibody on ice for 1h30. For competition experiments, cells were incubated with 15 μg/ml of the selected anti-HER4 mAbs and NRG1 at various concentrations (0.1 to 100 nM; 3 to 3000 ng/ml) on ice for 1h30. After washes, cells were incubated with FITC-conjugated goat anti-human IgG (Fc specific) (Sigma St-Louis, MI) or goat anti-mouse IgG (H+L) (Millipore). The cell median fluorescence intensity was measured by flow cytometry (Gallios apparatus, Beckman Coulter, Fullerton, CA).

2.6. HER4 binding by ELISA

Nunc MaxiSorp plates (Thermo Fisher) were coated with 250 ng/ml human or mouse recombinant HER4 overnight. After saturation at 37°C with PBS/2% BSA for 2h, antibodies were diluted in PBS/0.1% Tween and added for 2h at 37°C. After washes, antibody binding was detected by incubation with peroxidase-conjugated goat anti-human IgG (F(ab')2 fragment specific) (Jackson ImmunoResearch, West Grove, PA) and TMB solution. The reaction was stopped by adding 1M sulfuric acid, and absorbance was measured at 450 nm.

2.7. RT-PCR analysis of HER4 isoform expression

RT-PCR analysis of HER4 isoform expression was performed using appropriate primers, as described in Supporting Informations 1.

2.8. Mitochondrial activity measurement

Mitochondrial activity of C-33A cells was measured with the CellTiter 96 Aqueous One Solution Cell Proliferation Assay (MTS) (Promega, Madison, WI), as described in Supporting Informations 1.

2.9. Clonogenic survival

After trypsinization, six hundred C-33A cells were seeded in duplicate in 6-well plates in complete medium, 24h before antibody treatment (5μg/ml) or irradiation (1, 2 or 4Gy). At 15 days post-treatment, cells were fixed with 1:3 acetic acid/methanol solution and stained with Giemsa in water (3.5:10) (Sigma-Aldrich, St Louis, MO). Colonies containing at least 50 cells were counted, and the clonogenic survival was calculated as the number (x100) of colonies of surviving cells relative to untreated cells. As positive control, cells were irradiated with a linear particle accelerator (Varian Medical Systems; Palo Alto, CA) at the Radiotherapy Department of the ICM Val d'Aurelle hospital. Radiation was delivered as a single dose of 6MV-photons in a 40cm × 40cm field size at a dose rate of 200UM/min.

2.10. Adenylate kinase releasing assay

Adenylate kinase release from damaged cells was measured in HCC1187 cells using the ToxiLight Bioassay Kit (Lonza), as described in Supporting Informations 1.

2.11. ROS production

ROS level was measured in JMa/CYT1-, JMa/CYT2- and Mock-transfected BT549 cells using the DCFDA/H2DCFDA Cellular Reactive Oxygen Species Detection Assay Kit (Abcam, UK), as described in Supporting Informations 1.

2.12. Mitochondrial Membrane Potential

Mitochondrial Membrane Potential changes in JMa/CYT1-, JMa/CYT2- and Mock-transfected BT549 cells were evaluated using the DIOC6 intracellular probe (Abcam), as described in Supporting Informations 1.

2.13. Subcellular fractionation of BT549 transfected cells

BT549 transfected cells were stimulated or not with 30 ng/ml NRG1 at 37°C for 24h, or incubated with 20 μg/ml anti-HER4 antibodies in 1% FBS-medium, with or without 30 ng/ml NRG1 at 37°C for 6h. Subcellular fractionation of treated cells were performed as described in Supporting Informations 1.

2.14. Western blot analysis

Adherent cells were washed twice in cold PBS, dissociated by cell scraping, and lysed on ice in lysis buffer (60mM Tris pH 6.8, 10% glycerol (v/v), 1% SDS (v/v)). After boiling for 10min at 95°C, proteins were quantified and bromophenol blue added. 20-50 μg of protein lysates were separated by SDS-PAGE and then transferred onto PVDF membranes (GE Healthcare). Membranes were saturated in Tris Buffer Saline/0.1%Tween (TBS-T) and 5% non-fat dry milk with gentle shaking at room temperature for 2h. Membranes were incubated with rabbit or mouse primary antibodies at 4°C with gentle shaking overnight. After washes in TBS-T, membranes were incubated with the appropriate peroxidase-conjugated anti-mouse (Jackson ImmunoResearch) or anti-rabbit (Sigma) antibodies at room temperature for 1h. After washes in TBS-T, protein expression levels were detected with Western Lightening Ultra (Perkin Elmer) or SuperSignal West Femto Maximum Sensitivity Substrate (Thermo Fisher).

2.15. Epitope Mapping

The epitope mapping of C6 and D5 antibodies was predicted using MabTope software [31], as described in Supporting Informations 1. The amino acids that were identified as highly probable

epitope residues were mutated to alanine to create one mutated HER4 construct for each initially identified region. The wild type (HER4_WT) and mutated constructs (HER4_P1m, HER4_P2m, HER4_P3m and HER4_P4m) were N-terminally Flag-tagged to monitor antigen expression in HEK293 cells. The binding of C6 and D5 antibodies on wild type and mutated HER4-transfected HEK293 cells were performed by flow cytometry as described in Supporting Informations 1.

2.16. Tumor xenograft studies

All procedures were performed in compliance with the French regulations and ethical guidelines for experimental animal studies in an accredited establishment (Agreement No. C34-172-27). All experiments followed the relevant regulatory standards. Female Hsd nude mice were obtained from Envigo (Huntingdon, UK). At 6 weeks of age, mice were anesthetized and subcutaneously grafted with $8x10^6$ COV434 ovarian, $1x10^7$ C-33A cervical, or $1x10^7$ HCC1187 TNBC cells diluted in Matrigel solution (Corning, NY) in a final volume of 150 µl. Tumors were measured with a caliper twice a week to monitor size before and after treatment start. Once tumor size reached around 150 mm^3, mice were randomly distributed in groups of 10 mice and treatments started (intraperitoneal injections): irrelevant antibody (20 mg/kg), anti-HER4 D5 (20 mg/kg) and anti-HER4 C6 (20 mg/kg) twice per week for 4 weeks, or carboplatin (60 mg/kg) once per week for 4 weeks.

2.17. Immunohistochemistry (IHC)

Four-micron formalin-fixed, paraffin-embedded (FFPE) tissue sections from tumor xenografts were placed on poly-L-lysine coated slides, deparaffinized in xylene, and rehydrated in graded alcohols. The antigen retrieval was performed by heating tissues at 95°C in 10mM citrate buffer for 30min. The endogenous peroxidase activity was inhibited by Dual Endogenous Enzyme-Blocking Reagent for 15min (Dako, Glostrup, Denmark) and the nonspecific binding was reduced by the serum-free protein blocking (Dako) for 20min. The sections were then incubated with anti-cleaved caspase-3 antibody (Cell Signaling Technology, Beverly, MA)

diluted at 1:5000, for 1h. Antibody binding was revealed using the StreptaABComplex/HRP Duet kit (Dako). Quantification was done with the Aperio ImageScope software (Leica Biosystems. Wetzlar, Germany).

2.18. Statistical analysis

All statistical tests were performed using the Prism software v6.1 (GraphPad, San Diego, CA). Comparisons between groups were performed using the two-tailed unpaired Student's *t*-test. ANOVA was used for Figures 4D and S5. For all experiments, * is $p<0.05$, ** is $p<0.01$ and *** is $p<0.001$.

3. RESULTS

3.1. NRG1 induces cell death in HER4-expressing C-33A and COV318 cancer cells

We first studied the involvement of the NRG1/HER4 axis in tumor suppression in C-33A (cervical) and COV318 (ovary) cancer cell lines that strongly express HER4, but not HER3. These two cell lines also express EGFR and HER2 at different levels, as shown by flow cytometry (Fig. S1). Stimulation of C-33A cells with NRG1 induced stronger PARP cleavage over time, with regard to unstimulated cells, suggesting that cell death is triggered after HER4 activation by NRG1 (Fig. 1A). NRG1 also increased DNA fragmentation, as indicated by the finding that around 60% of NRG1-stimulated C-33A cells were in the sub-G1 phase at 48h-72h after addition of NRG1 (Fig. 1B). NRG1 also significantly decreased the metabolic activity (MTS assay) of C-33A cells (Fig. 1C), suggesting that NRG1-induced cell death occurs through mitochondria. Similarly, NRG1 stimulation of COV318 cells induced PARP cleavage (Fig. 1D) already at 24h-post NRG1 stimulation, and cell membrane disruption (Fig. 1E). We observed this “broken” phenotype also in HCC1187 TNBC cells that express HER4 (Fig. S2A), as confirmed by adenylate kinase release increase in the extracellular medium in NRG1-stimulated HCC1187 cells compared with untreated cells (Fig. S2B). These experiments demonstrated that the NRG1-HER4 axis induces cell death in C-33A, COV318 and HCC1187 cancer cells.

3.2. NRG1 induces cell death through the HER4 JMa/CYT1 isoform

It was previously demonstrated that 4ICD, after cleavage of the JMa/CYT1 or JMa/CYT2 isoform, favors apoptosis [19]. To determine which isoform is responsible for cell death after NRG1 stimulation, we transiently-transfected $HER3^{neg}/HER4^{neg}$ BT549 TNBC cells with plasmids that encode full-length HER4 JMa/CYT1 or JMa/CYT2. Flow cytometry analysis confirmed HER4 expression and showed that EGFR and HER2 expression were not affected by transfection (Fig. S3A). We also checked the expression of both full-length HER4 isoforms by western blotting (Fig. S3B), and the absence of expression in mock-transfected BT549 cells.

Expression of HER4 JMa/CYT1 was lower than that of JMa/CYT2 (Fig. S3B), in accordance with literature data [14,16]. RT-PCR analysis confirmed that non-transfected BT549 cells did not express any HER4 isoform (Fig. S3C).

In basal conditions (medium alone), the expression of each HER4 isoform in BT549 cells was sufficient to induce PARP cleavage at 48h post-transfection. Stimulation with NRG1 sustained PARP cleavage up to 72h in JMa/CYT1-transfected BT549 cells, but not in mock- and JMa/CYT2-transfected cells where PARP cleavage decreased (Fig. 2A). To confirm the opposite roles of HER4 JMa/CYT1 and JMa/CYT2, we overexpressed each isoform in C-33A cells. These cells naturally express the two isoforms at similar levels, but not the JMb isoforms (Fig. S3C). NRG1-induced PARP cleavage was comparable in parental and mock-transfected C-33A cells (compare Fig. 2B and Fig. 1A). HER4 JMa/CYT1 overexpression, but not JMa/CYT2 overexpression strongly induced PARP cleavage in unstimulated cells, particularly at 72h (Fig. 2B). Upon NRG1 stimulation, PARP cleavage was amplified from 48h onwards in HER4 JMa/CYT1-overexpressing C-33A cells, whereas it was decreased in JMa/CYT2-overexpressing cells, compared with NRG1-stimulated mock-cells (Fig. 2B).

3.3. NRG1-induced cell death through HER4 JMa/CYT1 occurs via JNK/γH2AX signaling

In $HER3^{neg}/HER4^{pos}$ C-33A cells, NRG1 stimulation decreased the cell metabolic activity (Fig. 1C) and promoted DNA fragmentation (Fig. 1B). Therefore, we wanted to identify the NRG1/HER4-related intermediates between mitochondria and PARP. It has been shown that sustained JNK activation induces apoptosis by interacting with mitochondrial proteins [32], and that NRG1 activates JNK through HER4 [33]. Moreover, HER4 is connected with DNA damage[34]. In agreement, NRG1 stimulation of mock-transfected C-33A cells increased JNK phosphorylation and the level of γH2AX (a marker of double-strand DNA breaks) over time (Fig. 2B), compared with unstimulated mock cells. In HER4 JMa/CYT1-overexpressing C-33A cells, JNK phosphorylation and γH2AX expression were induced earlier (24h vs 48h) and persisted until the experiment end (72h) in NRG1-stimulated compared with unstimulated cells

(Fig. 2B). Moreover, JNK phosphorylation level was lower in the absence of NRG1. Conversely, in HER4 JMa/CYT2-overexpressing C-33A cells, JNK phosphorylation was not induced in any condition (Fig. 2B), and basal γH2AX expression at 72h was reduced by NRG1 stimulation. These experiments confirmed that HER4 JMa/CYT1 acts as a tumor suppressor upon NRG1 stimulation, whereas JMa/CYT2 acts as a tumor protector.

3.4. NRG1 induces 4ICD retention in mitochondria of HER4 JMa/CYT1-transfected cells

As it has been shown that cleaved 4ICD closely interacts with mitochondria [19,21], we asked whether NRG1-induced cell death could be linked to 4ICD-CYT1 localization in mitochondria. To this aim, we investigated 4ICD localization in mitochondria and cytosol, after subcellular fractionation of JMa/CYT1 and JMa/CYT2-transfected BT549 cells. In non-stimulated cells (medium alone), we detected 4ICD in the mitochondrial fraction of HER4 JMa/CYT1- and JMa/CYT2-transfected BT549 cells (Fig. 3A). We also observed a pool of 4ICD-CYT1, but not of 4ICD-CYT2, in the cytosolic fraction of unstimulated cells. After NRG1 stimulation, full-length HER4 mostly disappeared both in the mitochondrial and cytosol fractions, suggesting increased HER4 degradation or shedding. Similarly, the mitochondrial fraction of 4ICD-CYT2, but not of 4ICD-CYT1 decreased (Fig. 3A). These results suggest that NRG1-induced cell death in HER4 JMa/CYT1-overexpressing cells occurs through 4ICD-CYT1 retention in mitochondria.

3.5. NRG1 induces ROS production following mitochondrial depolarization

ROS, the main cause of oxidative stress, is mainly produced in mitochondria, particularly upon sustained JNK activation [35]. Oxidative stress caused by ROS overproduction leads to DNA damage and cell death; however, a “sustained and controlled” ROS production could also favor tumor progression [36]. To investigate ROS role in HER4 JMa/CYT1-mediated cell death, we analyzed ROS production in transfected BT549 cells. Without NRG1 stimulation (Fig. 3B), ROS level was significantly higher in HER4 JMa/CYT1- and JMa/CYT2-transfected BT549

cells than in mock-transfected cells. As positive control, TBHP strongly induced ROS production. NRG1 stimulation significantly increased ROS production in HER4 JMa/CYT1- and JMa/CYT2-transfected BT549 cells, compared with unstimulated cells (only medium) (Fig. 3C). As ROS are mainly produced in mitochondria following reduction of the mitochondrial membrane potential, we used the DIOC6 probe to monitor the mitochondrial membrane potential. Flow cytometry analysis of DIOC6 labeled unstimulated HER4 JMa/CYT1- and JMa/CYT2-transfected BT549 cells demonstrated an increase of DIOC6 fluorescence signal, indicating mitochondrial membrane hyperpolarization, compared with mock-transfected cells (Fig. 3D). Conversely, NRG1 stimulation reduced DIOC6 labeling, indicating mitochondrial membrane depolarization (Fig. 3E). As positive control of depolarization, CCCP strongly reduced DIOC6 signal intensity. These results suggest that NRG1 induces ROS production following mitochondrial membrane depolarization of HER4 JMa/CYT1-expressing cells and participates in NRG1-induced cell death.

3.6. Selection and characterization of four anti-HER4 antibodies from the HUSCI phage-display library

Then, to select anti-HER4 antibodies that could mimic HER4 JMa/CYT1 tumor suppression *via* NRG1, we developed a whole cell panning approach in which we used HER4 JMa/CYT1-transfected NIH3T3 cells as targets (after stimulation with NRG1 to pre-activate HER4) and the proprietary phage display scFv library HUSCI (see Methods). We also performed a second phage display screening of the HUSCI library using soluble recombinant HER4 as target. Among the 400 clones screened by flow cytometry and ELISA, we selected and IgG1-reformatted four antibodies: D5, F4, and C6 (selected using the recombinant protein approach), and H2 (selected by whole cell panning). ELISA showed that the four antibodies bound to human HER4 in a dose-dependent manner (Fig. 4A). This binding was confirmed by flow cytometry in C-33A cells (Fig. S4A). D5 and C6, but not F4 and H2, cross-reacted with mouse HER4, as shown by ELISA (Fig. S4B). To assess HER4 specificity, we demonstrated that the selected antibodies D5, F4, C6 and H2 bound to EGFR/HER4 co-transfected 3T3

cells, but not to EGFR-only transfected 3T3 cells (Fig.S4C), and they did not cross-react with other ErbB family members, i.e. EGFR, HER2 and HER3 (Fig.S4D). The human HER4-specific D5 (10 ng/ml) and C6 (100 ng/ml) antibodies displayed 50% absorbance (EC50) on human HER4, and bound more efficiently than F4 and H2 (EC50 around 1-5 µg/ml) (Fig. 4A). Competition experiments using NRG1 and flow cytometry demonstrated that addition of low NRG1 concentrations (from 0.1 to 1 nM; 3 to 30 ng/ml) did not hinder antibody binding to HER4. D5 and F4 binding to HER4 was partially inhibited by 10 nM NRG1 (60% and 40% inhibition, respectively), but not C6 and H2 binding (Fig. 4B). F4 and H2, but not C6 and D5, still maintained around 40% of residual binding at high NRG1 concentration (100 nM).

We predicted the HER4 epitopes of the D5 and C6 antibodies using the MabTope software [31] (Fig. S5A-B). We identified four predicted areas that belong to the D5 and C6 putative epitopes: P1 606-623, P2 573-593, P3 260-279 and P4 622-642 (Fig. S5B), according to the numbering of the UniProtKB-Q15303 HER4 sequence. We designed HER4 mutants within the four predicted areas (HER4_P1m to P4m) (Fig. 4C) and transfected them in HEK293 cells. We mutated into alanine only surface residues, ensuring that HER4 structure was not altered. Flow cytometry analysis (Fig. S5C, and normalized data in Fig. 4D for C6 and D5) showed that the percentage of PE+/APC+ cells, which indicated HER4 expression at the cell surface and antibody binding, was increased in cells transfected with WT HER4 compared with mock-transfected cells. Compared with WT HER4-transfected cells, the percentage of double-positive cells was lower in HER4_P1m- and _P2m-transfected cells, whereas it was not significantly different in HER4_P3m- and _P4m-HER4-transfected cells (Fig. S5C and Fig. 4D). These results experimentally demonstrated that the anti-HER4 antibodies D5 and C6 share a common conformational epitope that is located in domain IV, close to the transmembrane region, and restricted to regions 605-620 (part of P1) and 575-592 (part of P2) (Fig. S5D).

3.7. Effect of the four selected antibodies on the metabolic activity and colony formation of C-33A cancer cells

To test the efficacy of the four anti-HER4 antibodies, we used an MTS assay to assess the metabolic activity of C-33A cells. Compared with control IgG (Ctrl), the metabolic activity of C-33A cells was reduced by 50% when incubated with D5 and by 15% to 30% in the presence of C6, F4 and H2 (Fig. 4E). Co-incubation with 10 ng/ml of NRG1 increased the C6-, F4- and H2-mediated metabolic activity inhibition to 50% (Fig. 4F), suggesting that NRG1 potentiates the effect of these antibodies. Conversely, NRG1 did not improve D5 inhibitory effect. The anti-HER4 agonist antibody Ab77 increased the metabolic activity of unstimulated and NRG1-stimulated C-33A cells up to 120%, as previously suggested [37]. To confirm, we analyzed the clonogenic survival of C-33A cells after treatment with anti-HER4 antibodies, to investigate whether selected antibodies could affect colony formation (Fig.4G). At day 15 post-treatment, the clonogenic survival was notably reduced in cells incubated with 5 μg/ml antibodies D5 and C6 than in cultures incubated with control IgG (Fig.4G; left panel). As positive controls, trastuzumab (Fig.4G; left panel), as well as dose-dependent irradiation (Fig.4G; right panel), also affected clonogenic survival of C-33A cells.

3.8. D5, C6 and H2, but not F4, induce 4ICD cleavage in HER4 JMa/CYT1-transfected cells

To test whether the four anti-HER4 antibodies could potentiate HER4 tumor suppressor activity, we first evaluated their ability to induce 4ICD cleavage in HER4 JMa/CYT1 and JMa/CYT2-transfected BT549 cells. We detected 4ICD by western blotting after incubation of JMa/CYT1-transfected cells with D5, C6 or H2 (Fig. 5A, left panel), suggesting that these antibodies promote JMa/CYT1 4ICD release. We did not observe 4ICD cleavage after incubation of JMa/CYT1-transfected BT549 cells with F4, and also after incubation of JMa/CYT2-transfected cells will the four antibodies (Fig. 5A, right panel). We then asked whether the antibodies activated HER4 through phosphorylation. D5 and C6, but not the anti-HER4 agonist Ab77, strongly induced HER4 phosphorylation on Y1056 in HER4 JMa/CYT1-

transfected BT549 cells, a phosphorylation site described as essential for HER4 tumor suppressor function [27] (Fig. 5B). Conversely, Ab77, but not D5 and C6, induced HER4 phosphorylation on Y984 in JMa/CYT1-transfected cells, a site responsible for 4ICD association with STAT5A [38]. No antibody-induced HER4 phosphorylation was observed in HER4 JMa/CYT2-transfected BT549 cells (Fig. 5B). These results suggest that the D5 and C6 mAbs induce HER4 ICD cleavage and HER4 phosphorylation via HER4 JMa/CYT1 activation.

3.9. The antibodies C6 and H2, but not D5 and F4, favor 4ICD retention in mitochondria in HER4 JMa/CYT1-transfected cells

We then asked whether the four anti-HER4 antibodies could induce 4ICD retention in mitochondria, as observed following NRG1 stimulation (Fig. 3A). C6 promoted 4ICD retention in mitochondria, as shown by western blotting after subcellular fractionation of HER4 JMa/CYT1-transfected BT549 cells (Fig. 5C; left panels), with and also without co-stimulation by NRG1. H2 promoted 4ICD retention in mitochondria, but only when NRG1 was added (Fig. 5C; left panels). Conversely, C6 and H2 did not have any effect on 4ICD retention in HER4 JMa/CYT2-transfected BT549 cells (Fig. 5C; right panels). This suggests that 4ICD routing to mitochondria is specific to cells that express the HER4 JMa/CYT1 isoform. D5 and F4 did not induce 4ICD retention in mitochondria in HER4 JMa/CYT1- and also JMa/CYT2-transfected BT549 cells (Fig. 5C). We then compared 4ICD localization induced by C6, which inhibited the metabolic activity of C-33A cells, and by the agonist Ab77 antibody, which increased metabolic activity (Fig. 4F). In HER4 JMa/CYT1-transfected BT549 cells, 4ICD-CYT1 retention in mitochondria was higher after incubation with C6 than with Ab77, as expected. Conversely, Ab77 favored 4ICD-CYT1 retention in the cytosol (Fig. 5D). This result shows that these two anti-HER4 mAbs can induce different signaling.

3.10. The agonist antibody C6 mimics NRG1-mediated effects on cell death, ROS production, and mitochondrial membrane depolarization

We then asked whether the four HER4-specific antibodies shared properties mediated by NRG1. In C-33A cells, C6 and D5 induced PARP cleavage after 72h of incubation (Fig. 6A) and γH2AX expression, indicating that they favored cell death by promoting double-strand DNA breaks. We confirmed these effects in COV318 cells (Fig. S6). C6, but not D5 induced mitochondrial membrane depolarization in HER4 JMa/CYT1-transfected BT549 cells (Fig. 6B), as observed with NRG1 (Fig. 3E). Conversely, incubation of mock- or HER4 JMa/CYT2-transfected BT549 cells with the two anti-HER4 antibodies did not induce any change in mitochondrial membrane potential (Fig. 6B), confirming that depolarization following 4ICD translocation into mitochondria is a specific mechanism to the HER4 JMa/CYT1 isoform. CCCP (positive control) induced mitochondrial membrane depolarization in mock-, JMa/CYT1- and JMa/CYT2-transfected BT549 cells. In addition, compared with mock-transfected cells, ROS production was slightly induced by C6 in HER4 JMa/CYT1-transfected BT549 cells (Fig. 6C, left and middle panels), and by D5 and C6 in JMa/CYT2 cells (Fig. 6C, right panel), suggesting that cancer cell death could be induced also via alternative mechanisms. Incubation with TBHP (positive control) induced ROS production in mock-, JMa/CYT1- and JMa/CYT2-transfected BT549 cells. These results indicate that the anti-HER4 antibody C6 is a cell death inducer that mimics NRG1-mediated effects in cancer cells.

3.11. In vivo the agonist C6 antibody reduces HER4^{pos} ovarian cancer and TNBC cell xenograft growth

Finally, we compared the antitumor efficacy *in vivo* of C6 (NRG1 agonist), D5 and carboplatin (positive control treatment). We xenografted athymic mice with COV434 ovarian cancer cells, C-33A cervical cancer cells and HCC1187 TNBC cells. At day 38 post-xenograft (3 days after the end of antibody treatment; day 35), COV434 cell tumor volume was significantly reduced by 33% in D5- and C6-treated mice ($p=0.04$ and $p=0.03$, respectively, compared with control IgG), and by 37% in carboplatin-treated animals ($p=0.01$) (Fig. 7A; higher panels). In

correlation, analysis of COV434 tumor samples at day 38 post-xenograft (exemplified in Fig.7A ; left lower panel) showed that the number of cancer cells positive for cleaved caspase-3 (a marker of apoptosis) tend to increase in mice treated with the anti-HER4 antibodies D5 and C6 compared with control-treated mice (Fig.7A ; right lower panel).

At day 41 post-xenograft, the mean tumor volume was reduced by 18% in mice xenografted with C-33A cells and treated with C6 compared with control (IgG), but this difference was not significant (p=0.617) (Fig. 7B). D5 did not affect tumor growth. Conversely, tumor volume was reduced by 59% (at day 38 post-graft) in mice treated with carboplatin (p=0.007). In mice xenografted with HCC1187 cells, tumor volume was reduced by 21.5% (at day 55 post-xenograft, 4 days after the treatment end; day 51) after treatment with C6 compared with control (IgG) (p=0.07) (Fig. 7C). D5 did not have any effect. At day 55 post-graft, tumor size was reduced by 54% in carboplatin-treated mice (p=0.001). These results demonstrate that the agonist anti-HER4 antibody C6 can delay tumor growth in mice xenografted with ovarian cancer or TNBC cells.

4. DISCUSSION

The development of antagonist mAbs is a classical and effective way to inhibit cancer progression (e.g. anti-EGFR and -HER2 antibodies). The characterization of anti-HER4 mAbs was initially based on the same concept: blocking HER4 activity to kill cancer cells [39]. However, HER4 is unique among the HER family members, with conflicting results concerning the relationship between patient survival and HER4 expression level [40]. Indeed, HER4 displays oncogenic or tumor suppressor activities, depending on the expression levels of its four isoforms [41]. In this context, the previously described anti-HER4 mAbs showed disappointing results because HER4 was targeted as a whole, thus blocking its oncogene and also tumor suppressor activities [42,43].

In this study, we characterized the pharmacological activity of four new anti-HER4 antibodies by focusing particularly on their effect on each HER4 isoform. The best antibody, C6, is a full agonist molecule that mimics NRG1 effects and promotes cleavage and retention of 4ICD in mitochondria, leading to antibody-induced cell death in HER4 JMa/CYT1-expressing cancer cells. Cell death occurred after ROS production through mitochondrial membrane depolarization, γH2AX expression due to DNA damage, and HER4 phosphorylation at Y1056. *In vivo*, C6 reduced tumor growth in mice xenografted with ovarian cancer or TNBC cells.

In $HER3^{neg}$ $HER4^{pos}$ C-33A cells, NRG1 induces PARP cleavage over time with DNA fragmentation by an unknown mechanism. PARP cleavage after NRG1 stimulation has been described in neurodegenerative diseases, and various cell death mechanisms can potentially be activated through HER4 [44]. We suspect an unconventional cell death mechanism (e.g. necroptosis or parthanatos) that involves endoplasmic reticulum stress. Indeed, protein level was increased after NRG1-induced cell death of HCC1187 cells, suggesting protein synthesis increase, as previously described [45]. Moreover, protein synthesis has been associated with ROS production and JNK activation [46], two events we detected in NGR1-stimulated HER4

JMa/CYT1-expressing cells. Protein synthesis could be also associated with parthanatos, a mitochondrial cell death that implicates ROS, AIF release, and PARP as central mediator [47].

The anti-tumor effect of the C6 antibody is related to HER4 JMa/CYT1 cleavage and formation of a stable active 4ICD fragment located in mitochondria. There are many evidences about HER4 tumor suppressor function through 4ICD, but the exact role of each isoform was never defined. We excluded JMb isoforms because they are not expressed in cancer and they are detected only in some tissues [6]. Using plasmids encoding the two full-length JMa isoforms, we demonstrated that NRG1-induced cell death occurred through HER4 JMa/CYT1. Conversely, HER4 JMa/CYT2 induced cell survival in BT549 cells, a TNBC model that initially does not express HER3 and HER4. Particularly, stimulation by NRG1 increased PARP cleavage in HER4 JMa/CYT1- but not in JMa/CYT2-transfected cells, highlighting the dichotomy between the tumor suppressor JMa/CYT1 isoform and the pro-survival JMa/CYT2 isoform. HER4 JMa/CYT1 acts by activating JNK, relocating 4ICD to the mitochondria and increasing ROS production. Altogether, these events lead to cell death, but we still have to precisely decipher the pathway. We hypothesized that ROS-induced DNA damage could be due to transient mitochondrial membrane potential changes, leading to a cell death mechanism called ROS-Induced ROS Release (RIRR), whereby ROS production is amplified in neighboring mitochondria [48]. Finally, *in vivo*, C6 inhibited growth of HCC1187 tumor cell xenografts (TNBC), possibly through is pro-apoptotic activity. As HER4 is expressed in about 20% of TNBC [41], a pathology still with unmet medical needs, targeting HER4 with agonist antibodies might represent an alternative strategy to treat TNBC.

We used this model as template for HER4 antibody discovery. As NRG1 induces cell death by activating HER4 JMa/CYT1, we tried to potentiate this function without hampering NRG1 action on HER4. To this end, we performed whole cell panning by phage display using NRG1-stimulated HER4 JMa/CYT1-transfected cells to select anti-HER4 mAbs with unique NRG1 agonist/modulator activity. First, NRG1 binding to HER4 differently affects mAb binding to the receptor. Using C-33A cells, we demonstrated that all selected mAbs can bind to HER4

in the presence of 30 ng/ml NRG1, a concentration that induces cancer cell death. Second, the selected mAbs act synergistically with NRG1 to decrease the cell metabolic activity. Third, the epitopes of C6 and D5 are far from the NRG1 binding site [49] on HER4, suggesting that cooperation between HER4-specific mAbs and NRG1 could occur at the cell surface.

Similarly to NRG1, C6 promotes HER4/4ICD localization in mitochondria, mitochondrial depolarization and ROS production, leading to cell death. These HER4 JMa/CYT1-triggered pathways suggest that the 16 aa stretch in CYT1 is crucial for cell death. Interestingly, the previously described anti-HER4 antibody MAb-3 [39] enhances apoptosis in HER4^{pos} non-small-cell lung carcinoma cells, with an increase of sub-diploid cells (a sign of DNA damage). Using the same MAb-3 antibody, Ben-Yosef et al. observed multiple apoptotic cells with pyknotic and fragmented nuclei, karyorrhexis, and loss of cytoplasm in prostate tumor xenograft sections from MAb-3-treated nude mice [50]. Breast cancer frequency is increased in HER4 JMa/CYT1 transgenic mice compared with HER4 JMa/CYT2 transgenic mice, with no apoptosis observed [9]. Thus, cell death induction seems to be a critical point for inhibiting tumorigenesis via HER4 [17]. We demonstrated that the C6 mAb efficiently kills ovarian cancer and TNBC cells *in vitro* by inducing PARP cleavage and DNA damage, and *in vivo* by reducing tumor growth. The anti-tumor effect of this new first-in-class anti-HER4 mAb must be confirmed in additional pre-clinical studies, especially in TNBC.

Finally, as the C6 mAb has a different binding site than NRG1 on HER4, our results suggest that similar pathways can be triggered from different receptor conformations, and indicate that C6 could be an allosteric modulator of HER4. Allosteric modulation is an important mechanism that has been recently adapted from small to large molecules [28,51]. By acting on the receptor, allosteric molecules can modulate endogenic ligand binding and/or signaling. C6 effect, combined with NRG1 binding on HER4, could exemplify allosteric modulation, with cooperation to initialize new signaling pathways through HER4 that cannot be activated by each molecule on its own. This phenomenon might implicate receptor rearrangement. The finding that C6, D5, Ab77 [37] and mAb1479 [52] have closely related epitopes but very different

mechanisms of action suggests that minor differences in conformational changes can induce major differences in signaling and cell fate. This study is the proof-of-concept that biased signaling can be induced with RTK-specific antibodies, as observed with GPCR-targeting molecules. Indeed, the C6 mAb localizes 4ICD in mitochondria, whereas the Ab77 mAb localizes 4ICD in the cytosol of HER4 JMa/CYT1-expressing cells, resulting in different cell fate. Altogether, our observations pave the way to novel mAbs with “biasing properties” for cancer treatment.

ACKNOWLEDGMENTS

We thank S. Bousquié (IRCM) for cell culture and T. David (IRCM) for antibody production. The staff members at the IRCM animal facility, the GenAc and MRI platforms, and the RHEM histology facility are greatly acknowledged. Y. Yarden (Weizmann Institute) is also greatly acknowledged for providing the anti-HER4 antibody Ab77. This work was supported by the program “Investissement d’Avenir” (grant agreement: Labex MAbImprove, ANR-10-LABX-53-01; A. Pèlegrin), by INSERM Transfert (CoPoC grant HER4Valid; T. Chardès). R. Lanotte was a recipient of a PhD studentship from the LabEx MAbImprove, and from the Ligue Nationale contre le Cancer. N. Gaborit was a recipient of a post-doctoral fellowship from the LabEx MAbImprove.

DISCLOSURE STATEMENT

R. Lanotte, P. Martineau, A. Pèlegrin and T. Chardès are inventors of the pending patent “Antibodies having specificity to HER4 and uses thereof”, The other authors declare no conflict of interest.

REFERENCES

1. Roskoski R. The ErbB/HER family of protein-tyrosine kinases and cancer. Pharmacol Res. 2014;79:34-74.
2. Lazrek Y, Dubreuil O, Garambois V, Gaborit N, Larbouret C, Le Clorennec C, et al. Anti-HER3 domain 1 and 3 antibodies reduce tumor growth by hindering HER2/HER3 dimerization and AKT-induced MDM2, XIAP, and FoxO1 phosphorylation. Neoplasia N Y N. 2013;15:335-47.
3. Hollmén M, Elenius K. Potential of ErbB4 antibodies for cancer therapy. Future Oncol Lond Engl. 2010;6:37-53.
4. Kim J-Y, Jung HH, Do I-G, Bae S, Lee SK, Kim SW, et al. Prognostic value of ERBB4 expression in patients with triple negative breast cancer. BMC Cancer. 2016;16:138.
5. Wang J, Yin J, Yang Q, Ding F, Chen X, Li B, et al. Human epidermal growth factor receptor 4 (HER4) is a favorable prognostic marker of breast cancer: a systematic review and meta-analysis. Oncotarget. 2016;7:76693-703.
6. Veikkolainen V, Vaparanta K, Halkilahti K, Iljin K, Sundvall M, Elenius K. Function of ERBB4 is determined by alternative splicing. Cell Cycle Georget Tex. 2011;10:2647-57.
7. Ni CY, Murphy MP, Golde TE, Carpenter G. gamma -Secretase cleavage and nuclear localization of ErbB-4 receptor tyrosine kinase. Science. 2001;294:2179-81.
8. Haskins JW, Nguyen DX, Stern DF. Neuregulin 1-activated ERBB4 interacts with YAP to induce Hippo pathway target genes and promote cell migration. Sci Signal. 2014;7:ra116.
9. Wali VB, Gilmore-Hebert M, Mamillapalli R, Haskins JW, Kurppa KJ, Elenius K, et al. Overexpression of ERBB4 JM-a CYT-1 and CYT-2 isoforms in transgenic mice reveals isoform-specific roles in mammary gland development and carcinogenesis. Breast Cancer Res BCR. 2014;16:501.
10. Kainulainen V, Sundvall M, Määttä JA, Santiestevan E, Klagsbrun M, Elenius K. A natural ErbB4 isoform that does not activate phosphoinositide 3-kinase mediates proliferation but not survival or chemotaxis. J Biol Chem. 2000;275:8641-9.
11. Xu S, Kitayama J, Yamashita H, Souma D, Nagawa H. Nuclear translocation of HER-4/c-erbB-4 is significantly correlated with prognosis of esophageal squamous cell carcinoma. J Surg Oncol. 2008;97:44-50.
12. Paatero I, Lassus H, Junttila TT, Kaskinen M, Bützow R, Elenius K. CYT-1 isoform of ErbB4 is an independent prognostic factor in serous ovarian cancer and selectively promotes ovarian cancer cell growth in vitro. Gynecol Oncol. 2013;129:179-87.
13. Sundvall M, Korhonen A, Paatero I, Gaudio E, Melino G, Croce CM, et al. Isoform-specific monoubiquitination, endocytosis, and degradation of alternatively spliced ErbB4 isoforms. Proc Natl Acad Sci U S A. 2008;105:4162-7.
14. Sundvall M, Peri L, Määttä JA, Tvorogov D, Paatero I, Savisalo M, et al. Differential nuclear localization and kinase activity of alternative ErbB4 intracellular domains. Oncogene. 2007;26:6905-14.
15. Bae JA, Kho DH, Sun EG, Ko Y-S, Yoon S, Lee KH, et al. Elevated Coexpression of KITENIN and the ErbB4 CYT-2 Isoform Promotes the Transition from Colon Adenoma

to Carcinoma Following APC loss. Clin Cancer Res Off J Am Assoc Cancer Res. 2016;22:1284-94.

16. Määttä JA, Sundvall M, Junttila TT, Peri L, Laine VJO, Isola J, et al. Proteolytic cleavage and phosphorylation of a tumor-associated ErbB4 isoform promote ligand-independent survival and cancer cell growth. Mol Biol Cell. 2006;17:67-79.
17. Wali VB, Haskins JW, Gilmore-Hebert M, Platt JT, Liu Z, Stern DF. Convergent and divergent cellular responses by ErbB4 isoforms in mammary epithelial cells. Mol Cancer Res MCR. 2014;12:1140-55.
18. Muraoka-Cook RS, Sandahl MA, Strunk KE, Miraglia LC, Husted C, Hunter DM, et al. ErbB4 splice variants Cyt1 and Cyt2 differ by 16 amino acids and exert opposing effects on the mammary epithelium in vivo. Mol Cell Biol. 2009;29:4935-48.
19. Naresh A, Long W, Vidal GA, Wimley WC, Marrero L, Sartor CI, et al. The ERBB4/HER4 intracellular domain 4ICD is a BH3-only protein promoting apoptosis of breast cancer cells. Cancer Res. 2006;66:6412-20.
20. Thor AD, Edgerton SM, Jones FE. Subcellular localization of the HER4 intracellular domain, 4ICD, identifies distinct prognostic outcomes for breast cancer patients. Am J Pathol. 2009;175:1802-9.
21. Schumacher MA, Hedl M, Abraham C, Bernard JK, Lozano PR, Hsieh JJ, et al. ErbB4 signaling stimulates pro-inflammatory macrophage apoptosis and limits colonic inflammation. Cell Death Dis. 2017;8:e2622.
22. Jones FE. HER4 intracellular domain (4ICD) activity in the developing mammary gland and breast cancer. J Mammary Gland Biol Neoplasia. 2008;13:247-58.
23. Das PM, Thor AD, Edgerton SM, Barry SK, Chen DF, Jones FE. Reactivation of epigenetically silenced HER4/ERBB4 results in apoptosis of breast tumor cells. Oncogene. 2010;29:5214-9.
24. Muraoka-Cook RS, Sandahl M, Husted C, Hunter D, Miraglia L, Feng S, et al. The intracellular domain of ErbB4 induces differentiation of mammary epithelial cells. Mol Biol Cell. 2006;17:4118-29.
25. Strunk KE, Husted C, Miraglia LC, Sandahl M, Rearick WA, Hunter DM, et al. HER4 D-box sequences regulate mitotic progression and degradation of the nuclear HER4 cleavage product s80HER4. Cancer Res. 2007;67:6582-90.
26. Chua YL, Ito Y, Pole JCM, Newman S, Chin S-F, Stein RC, et al. The NRG1 gene is frequently silenced by methylation in breast cancers and is a strong candidate for the 8p tumour suppressor gene. Oncogene. 2009;28:4041-52.
27. Gallo RM, Bryant I, Fry R, Williams EE, Riese DJ. Phosphorylation of ErbB4 on Tyr1056 is critical for inhibition of colony formation by prostate tumor cell lines. Biochem Biophys Res Commun. 2006;349:372-82.
28. Webb DR, Handel TM, Kretz-Rommel A, Stevens RC. Opportunities for functional selectivity in GPCR antibodies. Biochem Pharmacol. 2013;85:147-52.
29. Yea K, Zhang H, Xie J, Jones TM, Yang G, Song BD, et al. Converting stem cells to dendritic cells by agonist antibodies from unbiased morphogenic selections. Proc Natl Acad Sci U S A. 2013;110:14966-71.

30. Robin G, Sato Y, Desplancq D, Rochel N, Weiss E, Martineau P. Restricted diversity of antigen binding residues of antibodies revealed by computational alanine scanning of 227 antibody-antigen complexes. J Mol Biol. 2014;426:3729-43.
31. Bourquard T, Musnier A, Puard V, Tahir S, Ayoub MA, Jullian Y, et al. MAbTope: A Method for Improved Epitope Mapping. J Immunol Baltim Md 1950. 2018;201:3096-105.
32. Wagner EF, Nebreda AR. Signal integration by JNK and p38 MAPK pathways in cancer development. Nat Rev Cancer. 2009;9:537-49.
33. Muraoka-Cook RS, Caskey LS, Sandahl MA, Hunter DM, Husted C, Strunk KE, et al. Heregulin-dependent delay in mitotic progression requires HER4 and BRCA1. Mol Cell Biol. 2006;26:6412-24.
34. Gilmore-Hebert M, Ramabhadran R, Stern DF. Interactions of ErbB4 and Kap1 connect the growth factor and DNA damage response pathways. Mol Cancer Res MCR. 2010;8:1388-98.
35. Festjens N, Vanden Berghe T, Vandenabeele P. Necrosis, a well-orchestrated form of cell demise: signalling cascades, important mediators and concomitant immune response. Biochim Biophys Acta. 2006;1757:1371-87.
36. Chio IIC, Tuveson DA. ROS in Cancer: The Burning Question. Trends Mol Med. 2017;23:411-29.
37. Chen X, Levkowitz G, Tzahar E, Karunagaran D, Lavi S, Ben-Baruch N, et al. An immunological approach reveals biological differences between the two NDF/heregulin receptors, ErbB-3 and ErbB-4. J Biol Chem. 1996;271:7620-9.
38. Han W, Sfondouris ME, Jones FE. Direct coupling of the HER4 intracellular domain (4ICD) and STAT5A signaling is required to induce mammary epithelial cell differentiation. Biochem Biophys Rep. 2016;7:323-7.
39. Starr A, Greif J, Vexler A, Ashkenazy-Voghera M, Gladesh V, Rubin C, et al. ErbB4 increases the proliferation potential of human lung cancer cells and its blockage can be used as a target for anti-cancer therapy. Int J Cancer. 2006;119:269-74.
40. Bièche I, Onody P, Tozlu S, Driouch K, Vidaud M, Lidereau R. Prognostic value of ERBB family mRNA expression in breast carcinomas. Int J Cancer. 2003;106:758-65.
41. Machleidt A, Buchholz S, Diermeier-Daucher S, Zeman F, Ortmann O, Brockhoff G. The prognostic value of Her4 receptor isoform expression in triple-negative and Her2 positive breast cancer patients. BMC Cancer. 2013;13:437.
42. Hollmén M, Määttä JA, Bald L, Sliwkowski MX, Elenius K. Suppression of breast cancer cell growth by a monoclonal antibody targeting cleavable ErbB4 isoforms. Oncogene. 2009;28:1309-19.
43. Okazaki S, Nakatani F, Masuko K, Tsuchihashi K, Ueda S, Masuko T, et al. Development of an ErbB4 monoclonal antibody that blocks neuregulin-1-induced ErbB4 activation in cancer cells. Biochem Biophys Res Commun. 2016;470:239-44.
44. Fricker M, Tolkovsky AM, Borutaite V, Coleman M, Brown GC. Neuronal Cell Death. Physiol Rev. 2018;98:813-80.

45. Han J, Back SH, Hur J, Lin Y-H, Gildersleeve R, Shan J, et al. ER-stress-induced transcriptional regulation increases protein synthesis leading to cell death. Nat Cell Biol. 2013;15:481-90.
46. Urano F, Wang X, Bertolotti A, Zhang Y, Chung P, Harding HP, et al. Coupling of stress in the ER to activation of JNK protein kinases by transmembrane protein kinase IRE1. Science. 2000;287:664-6.
47. Fatokun AA, Dawson VL, Dawson TM. Parthanatos: mitochondrial-linked mechanisms and therapeutic opportunities. Br J Pharmacol. 2014;171:2000-16.
48. Zorov DB, Juhaszova M, Sollott SJ. Mitochondrial ROS-induced ROS release: an update and review. Biochim Biophys Acta. 2006;1757:509-17.
49. Liu P, Cleveland TE, Bouyain S, Byrne PO, Longo PA, Leahy DJ. A single ligand is sufficient to activate EGFR dimers. Proc Natl Acad Sci U S A. 2012;109:10861-6.
50. Ben-Yosef R, Starr A, Karaush V, Loew V, Lev-Ari S, Barnea I, et al. ErbB-4 may control behavior of prostate cancer cells and serve as a target for molecular therapy. The Prostate. 2007;67:871-80.
51. Wootten D, Christopoulos A, Sexton PM. Emerging paradigms in GPCR allostery: implications for drug discovery. Nat Rev Drug Discov. 2013;12:630-44.
52. Hollmén M, Liu P, Kurppa K, Wildiers H, Reinvall I, Vandorpe T, et al. Proteolytic processing of ErbB4 in breast cancer. PloS One. 2012;7:e39413.

FIGURE LEGENDS

FIGURE 1. NRG1 induces cell death in HER4-expressing C-33A and COV318 cancer cells. (**A**) C-33A cervical cancer cells were serum-starved for 12h, stimulated with NRG1 (30 ng/ml) for the indicated times and analyzed by western blotting using the appropriate antibodies. Western blots were repeated two times independently. Pixel intensity (PI) of each band was quantified using the Image J software. (**B**) C-33A cells were treated in triplicate as described in (A), stained with propidium iodide and analyzed by flow cytometry. Experiments were performed twice. *p<0.05, ***p<0.001 (unpaired t test) (**C**) Triplicate wells of C-33A cells were serum-starved for 12h and stimulated with NRG1 (30 ng/ml) for 5 days. Metabolic activity was analyzed with the MTS assay. Data are representative of two independent experiments and are presented as mean±SEM. **p<0.01, (unpaired t test). (**D**) COV318 ovary cancer cells were serum-starved for 12h, stimulated with NRG1 (30 ng/ml) for 24h and analyzed by western blotting in one experiment using the appropriate antibodies. Pixel intensity (PI) of each band was quantified using the Image J software. (**E**) Photographs (microscopy magnification: x10) showing the phenotype of unstimulated cells (top) and NRG1-stimulated COV318 cells (bottom). Representative microphotographs are shown (n=3).

FIGURE 2. NRG1 induces cell death through the HER4 JMa/CYT1 isoform and JNK/γH2AX signaling. (**A**) BT549 TNBC cells were transfected with plasmids encoding full-length HER4 JMa/CYT1 or JMa/CYT2, or Mock-transfected. At 24h post-transfection, cells were serum-starved for 12h, stimulated or not with NRG1 (30 ng/ml) for the indicated times and analyzed by western blotting using the appropriate antibodies. Pixel intensity (PI) of each band was quantified using the Image J software. (**B**) C-33A cells that naturally express both HER4 JMa isoforms were transfected with plasmids encoding full-length HER4 JMa/CYT1 or JMa/CYT2, or Mock-transfected. At 24h post-transfection, cells were serum-starved for 12h, stimulated or not with NRG1 (30 ng/ml) for the indicated times and analyzed by western blotting using the

appropriate antibodies. All experiments were carried out two times and representative blots are shown.

FIGURE 3. In HER4 JMa/CYT1-transfected cells, NRG1 induces 4ICD retention in mitochondria and ROS production through mitochondrial depolarization. (**A**) Subcellular fractionation of BT549 cells transfected with HER4 JMa/CYT1- or JMa/CYT2-encoding plasmids for 5h, serum-starved for 19h, and stimulated or not (Medium) with NRG1 (30 ng/ml) for 24h. The cytosol and mitochondrial fractions were identified with antibodies against α-tubulin and TIM23, respectively. The localization of full-length HER4 and 4ICD was assessed using the anti-HER4 antibody E200 (Abcam) that recognize full-length HER4 (180 kDa) and 4ICD (80 kDa). Western blots were repeated two times independently. WCL: Whole Cell Lysate. (**B**) ROS quantification in HER4 JMa/CYT1- and JMa/CYT2-transfected BT549 cells vs Mock-transfected cells. At 24h post-transfection in duplicate, cells were serum-starved for 18h, and ROS levels were quantified with the Cellular Reactive Oxygen Species Detection Assay Kit (Abcam). The ROS-inducer TBHP was used as positive control. Data are expressed as mean±SEM and are representative of two experiments. *p<0.05, **p<0.01 (unpaired t test). RLU: Relative Luminescence Unit. (**C**) ROS measurement after NRG1 stimulation of HER4 JMa/CYT1- and JMa/CYT2-transfected BT549 cells. At 24h post-transfection in duplicate, cells were serum-starved for 12h and then stimulated or not (M) with NRG1 (30 ng/ml) for 24h. ROS levels were quantified as in (B). Data are expressed as mean±SEM and are representative of two independent experiments. *p<0.05, ***p<0.001 (unpaired t test). RLU: Relative Luminescence Unit. (**D**) Mitochondrial Membrane Potential (MMP) measurement of HER4 JMa/CYT1 and JMa/CYT2-transfected BT549 cells vs Mock-transfected cells. At 24h post-transfection, cells were serum-starved for 12h and MMP was analyzed by flow cytometry using the DIOC6 probe. The assay was repeated two times independently. (**E**) MMP measurement after NRG1 stimulation of HER4 JMa/CYT1 and JMa/CYT2-transfected BT549 cells. At 24h post-transfection, cells were serum-starved for 12h and then stimulated or not with NRG1 (30

ng/ml) for 24h. Two independent experiments were performed and MMP was measured as in (D). The mitochondrial oxidative phosphorylation uncoupler CCCP was used as positive control for mitochondrial membrane depolarization.

FIGURE 4. Selection and characterization of four anti-HER4 antibodies from the HUSCI phage-display library. (**A**) ELISA binding of the selected mAbs to human HER4. Wells were coated with 250 ng/ml of recombinant HER4, and 20 μg/ml of mAbs was used in triplicate as starting concentration (1:10 dilution). Ipilimumab was used as negative control antibody. The assay was repeated two times (**B**) Effect of NRG1 on antibody binding to $HER4^{pos}$ C-33A cells assessed by flow cytometry. Cells were co-incubated with D5, F4, C6 or H2 (15 μg/ml) and various NRG1 concentrations. Results are presented as percentage of binding relative to the binding without NRG1 (M; 100%) for one experiment. (**C**) HER4 variants with mutations within the four predicted areas (HER4_P1 to P4). Only amino-acids from the HER4 protein surface were mutated to alanine, to ensure that HER4 structure was not altered. All wild type (WT) and mutants were N-terminally Flag-tagged and transfected in HEK293 cells, as described in the Materials and Methods section. (**D**) Binding of the anti-HER4 antibodies C6 and D5 in Mock, WT HER4 and HER4 mutant-transfected HEK293 cells. The number of APC+PE+ double-positive cells was quantified by flow cytometry, and normalized to the total number of PE+ cells within the sample. Duplicate wells were done for each condition. Data are representative of three independent experiments. ***$p<0.001$ (ANOVA test). n.s: non-significant. (**E**) Effect of the four anti-HER4 mAbs on the metabolic activity of C-33A cells. At 24h post-seeding, cells were incubated in triplicate with D5, F4, C6, H2 or Ab77 (100 μg/ml) for 5 days. Metabolic activity was analyzed using the MTS assay and presented as percentage of the activity in untreated cells (100%). Ctrl: negative control antibody. (**F**) Effect of the four anti-HER4 mAbs on the metabolic activity of NRG1-stimulated C-33A cells. At 24h post-seeding, cells were serum-starved for 12h and then co-incubated in triplicate with D5, F4, C6, H2 or Ab77 (100 μg/ml) and NRG1 (10 ng/ml) for 5 days. Metabolic activity was analyzed as in (E). Ctrl: negative

control antibody. Data in (E) and (F) are representative of two independent experiments and are the mean±SEM. (**G**) Percent clonogenic survival (Giemsa staining) of C-33A cells at day 15 after exposure to 5μg/ml anti-HER4 mAbs, trastuzumab (Tz) or dose-dependent (1 to 4Gy) irradiation. Colonies containing at least 50 cells were counted in the whole P6 wells done in duplicate for one experiment, and the clonogenic survival was calculated as the number (x100) of colonies of surviving cells relative to untreated cells. *p<0.05, **p<0.01, ***p<0.001 (unpaired t test). n.s: non-significant.

FIGURE 5. Anti-HER4 antibodies favor 4ICD release and HER4 phosphorylation, leading to 4ICD retention into mitochondria. (**A**) D5, C6 and H2, but not F4 induce 4ICD cleavage from HER4 JMa/CYT1-transfected BT549 cells. At 24h post-transfection with the HER4 JMa/CYT1 or JMa/CYT2 plasmid, cells were incubated with the indicated antibodies (20 μg/ml) for 24h. Full-length HER4 and 4ICD levels were analyzed by western blotting using the anti-HER4 antibody E200 (Abcam) that recognizes full-length HER4 (180 kDa) and 4ICD (80 kDa). (**B**) D5 and C6, but not Ab77, induce HER4 phosphorylation at Y1056 in HER4 JMa/CYT1-transfected BT549 cells. At 24h post-transfection, cells were serum-starved for 12h and incubated with the indicated mAbs (20 μg/ml) for 1h30. HER4 phosphorylation on Y984 and Y1056, and full-length HER4 were analyzed by western blotting using appropriate antibodies. (**C**) C6 and H2, but not D5 and F4, favor 4ICD retention in mitochondria of HER4 JMa/CYT1-transfected BT549 cells. Cells were transfected with HER4 JMa/CYT1 (left panel) or JMa/CYT2 (right panel) plasmids for 5h, serum-starved for 19h, and then stimulated or not with NRG1 and incubated with 20 μg/ml anti-HER4 antibodies for another 6h. After subcellular fractionation, the cytosolic and mitochondrial fractions were confirmed with antibodies against α-tubulin, and VDAC1 or TIM23, respectively. HER4 and 4ICD localizations were detected using the anti-HER4 antibody E200 (Abcam). WCL: Whole Cell Lysate. (**D**) Subcellular fractionation of HER4 JMa/CYT1-transfected BT549 cells incubated with C6 or Ab77 (20 μg/ml) for 6h. Cells were analyzed as in (B) and (C), with TFAM as mitochondrial fractionation

control. All experiments were repeated at least two times independently and representative blots are shown. Pixel intensity (PI) of each band was quantified using the Image J software.

FIGURE 6. The agonist antibody C6 mimics NRG1-mediated effects on cell death, ROS production, and mitochondrial membrane depolarization. (**A**) C-33A cells were incubated with D5 and C6 (20 μg/ml) for the indicated times and then analyzed by western blotting. The assay was repeated two times. (**B**) MMP measurement after incubation with D5 and C6 of Mock-, HER4 JMa/CYT1- and JMa/CYT2-transfected BT549 cells. At 24h post-transfection, cells were serum-starved for 12h and then incubated with antibodies (20 μg/ml) for 24h. MMP was measured using the DIOC6 probe. The experiment was repeated two times independently and representative cytometry profiles are shown. CCCP was used as positive control. Ctrl: negative control antibody. (**C**) ROS quantification after incubation with D5 and C6 of Mock-, HER4 JMa/CYT1- and JMa/CYT2-transfected BT549 cells. At 24h post-transfection, cells were serum-starved for 12h and then incubated in duplicate with antibodies (20 μg/ml) for 24h. TBHP was used as positive control. The assay was carried two times independently and representative histograms are shown. M: medium. Ctrl: negative control antibody. *$p<0.05$ (unpaired t test).

FIGURE 7. The agonist antibody C6 reduces *in vivo* tumor growth of HER4^{pos} ovarian cancer and TNBC cells. Nude mice (n=10/condition) were xenografted with COV434 ovarian cancer cells (**A;** upper panels), C-33A cervical cancer cells (**B**), or HCC1187 TNBC cells (**C**). When tumors reached a volume of 150 mm^3, mice were treated by intraperitoneal injection of 20 mg/kg of D5 (open white circles) and C6 (open white triangles) (anti-HER4 antibodies), or control antibody (full black squares), twice per week for 4 weeks. Carboplatin (full black triangles; positive control) was used at 60 mg/kg, once per week for 4 weeks. Tumor growth data are presented as the mean tumor volume±SEM for each group (left panels). The tumor size of each individual mouse is indicated at the end of treatment (right panel). n.s.: non-

significant. (**A;** left lower panel) Immunohistochemistry staining (20X magnification) of cleaved caspase-3 expression in COV434 sections from xenografted mice at day 38 of treatment. For each condition, FFPE tissue sections prepared from five extracted xenografts were stained independently and representative staining are shown. (**A;** right lower panel). For each treatment, cleaved caspase 3 intensity was quantified with Image Scope in the whole stained FFPE tissue section (n=5/condition).

SUPPORTING INFORMATIONS 1

Materials and Methods

Table S1. References of reagents and resources used in this study

SUPPORTING INFORMATIONS 2

FIGURE S1. Flow cytometry analysis of HER receptor expression in C-33A cervical cancer cells (**A**), and COV318 ovary cancer cells (**B**) in one experiment. Ctrl: negative control antibody.

FIGURE S2. (**A**) Microphotographs (microscopy magnification: x40) of unstimulated and NRG1-stimulated HCC1187 TNBC cells. Representative microphotographs are shown (n=3). (**B**) Adenylate kinase (AK) release from unstimulated and NRG1-stimulated HCC1187 cells. Cells were serum-starved for 12h, and stimulated or not with NRG1 in sextuplicate for 72h. Then, cell death was analyzed using an AK-releasing assay. Experiments were repeated two times independently and data are represented as mean±SEM. **p<0.01 (unpaired t test).

FIGURE S3. (**A**) Flow cytometry analysis of HER expression in Mock-, HER4 JMa/CYT1- and JMa/CYT2-transfected BT549 cells in one experiment. Ctrl: negative control antibody. (**B**) Western blot analysis of HER4 and 4ICD expression in parental (wt), mock-, HER4 JMa/CYT1- and JMa/CYT2-transfected BT549 cells using the E200 antibody that recognizes both full-length HER4 (180 kDa) and 4ICD (80 kDa). The experiments were carried out two times independently and representative blots are shown. GAPDH was used as loading control. (**C**) RT-PCR analysis of HER4 isoform expression in non-transfected BT549 (TNBC) cells and C-33A (cervical cancer) cells. The experiments were performed twice.

FIGURE S4. (**A**) Flow cytometry analysis of the binding of the selected antibodies D5, F4, C6 and H2 in C-33A cancer cells. Analysis was carried out two times independently and representative cytometry profiles are shown. Ctrl IgG: negative control antibody. (**B**) ELISA analysis of the binding of the selected anti-HER4 antibodies to mouse recombinant HER4. Ipilimumab was used as negative control antibody (Ctrl IgG). Triplicate wells were set up for each antibody dilution. (**C**) Flow cytometry binding of the selected anti-HER4 antibodies to

EGFR/HER4 co-transfected vs EGFR-only transfected 3T3 cells. The experiments were repeated three times and representative cytometry profiles are shown. (**D**) ELISA binding of 2μg/ml concentration of selected anti-HER4 antibodies to ErbB family members EGFR, HER2, HER3 and HER4. Triplicate wells were set up for each antibody dilution. Ctrl IgG: negative control antibody.

FIGURE S5. D5 and C6 epitope characterization using the MabTope technology. (**A**) Prediction of the best positions for the D5 and C6 epitope using the MabTope *in silico* method. D5 and C6 3D-structures were modeled, docked on HER4 (PDB:2AHX), and $5x10^8$ conformational positions were generated for the complexes. The view of the top 30 ranked predicted conformations for the complex between C6 and D5 (in colors) and the HER4 structure (in grey) is presented. (**B**) Probability for HER4 residue implication in the D5 and C6 epitopes. For each mAb, the frequency of each residue in the epitope was evaluated from the 30 best predicted interfaces. Frequency is represented in blue (darker color indicates higher probability for the residue to be implicated in the epitope). Four regions in HER4 ECD (P1 to P4) appeared to be implicated in mAb binding. (**C**) Flow cytometry analysis of C6 and D5 binding in mock-, WT HER4-, HER4 mutant (P1m-, P2m-, P3m- and P4m)-transfected HEK293 cells. Each HER4 variant harbors a mutation in one of the four predicted regions (HER4_P1m to P4m) (Figure 4C). After cell fixation, membrane HER4 expression was monitored with the PE-coupled anti-Flag antibody (ordinate), and C6 or D5 binding was measured with an APC-coupled anti-IgG antibody (abscissa). An irrelevant IgG was used as control (Ctrl). Duplicate wells were done for each condition. Data are representative of three independent experiments. (**D**) Localization of the regions 575-592 and 605-620 (involved in the conformational epitopes of anti-HER4 antibodies C6 and D5) on the HER4 crystallographic structure (PDB:2AHX).

FIGURE S6. Western blot analysis of COV318 cells incubated with the D5 and C6 mAbs for the indicated times. In one experiment, cleaved PARP, γH2AX, HER4 and 4ICD were detected using the appropriate primary antibodies.

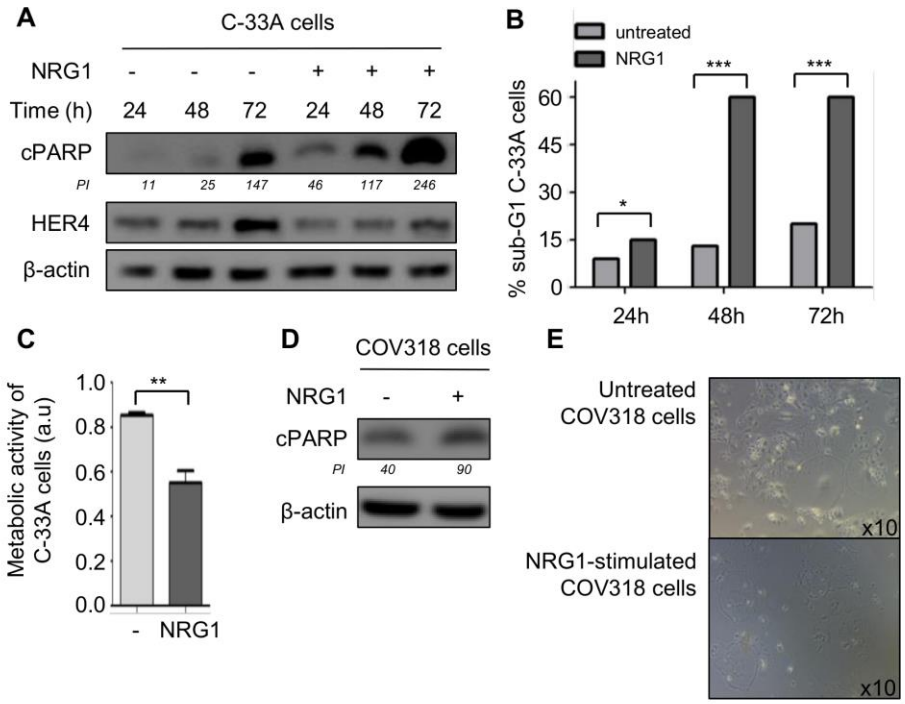
A
C-33A cells
NRG1 - - - + + +
Time (h) 24 48 72 24 48 72
cPARP
PI 11 25 147 46 117 246
HER4
β-actin
B
untreated
NRG1
% sub-G1 C-33A cells
60
45
30
15
0
*
***
***
24h
48h
72h
C
Metabolic activity of C-33A cells (a.u)
1.0
0.8
0.6
0.4
0.2
0.0
**
- NRG1
D
COV318 cells
NRG1 - +
cPARP
PI 40 90
β-actin
E
Untreated COV318 cells
x10
NRG1-stimulated COV318 cells
x10

Figure 1

1

2

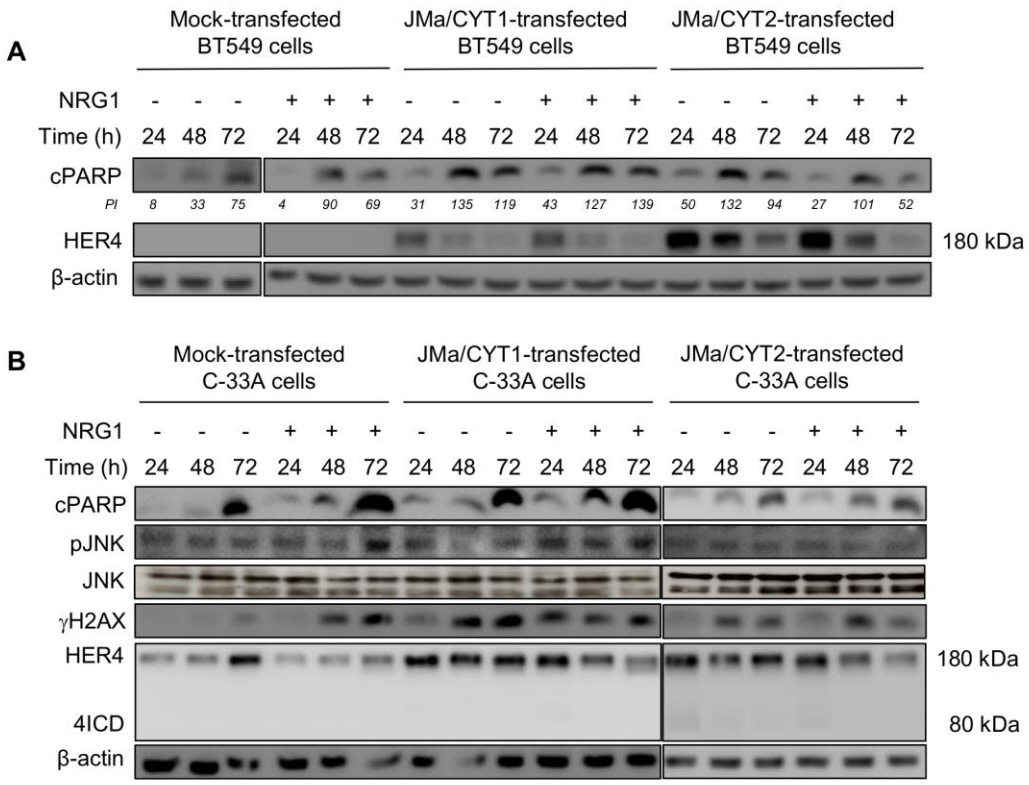
A
Mock-transfected BT549 cells
JMa/CYT1-transfected BT549 cells
JMa/CYT2-transfected BT549 cells
NRG1
Time (h)
cPARP
PI
HER4
β-actin
180 kDa
B
Mock-transfected C-33A cells
JMa/CYT1-transfected C-33A cells
JMa/CYT2-transfected C-33A cells
NRG1
Time (h)
cPARP
pJNK
JNK
γH2AX
HER4
4ICD
β-actin
180 kDa
80 kDa

Figure 2

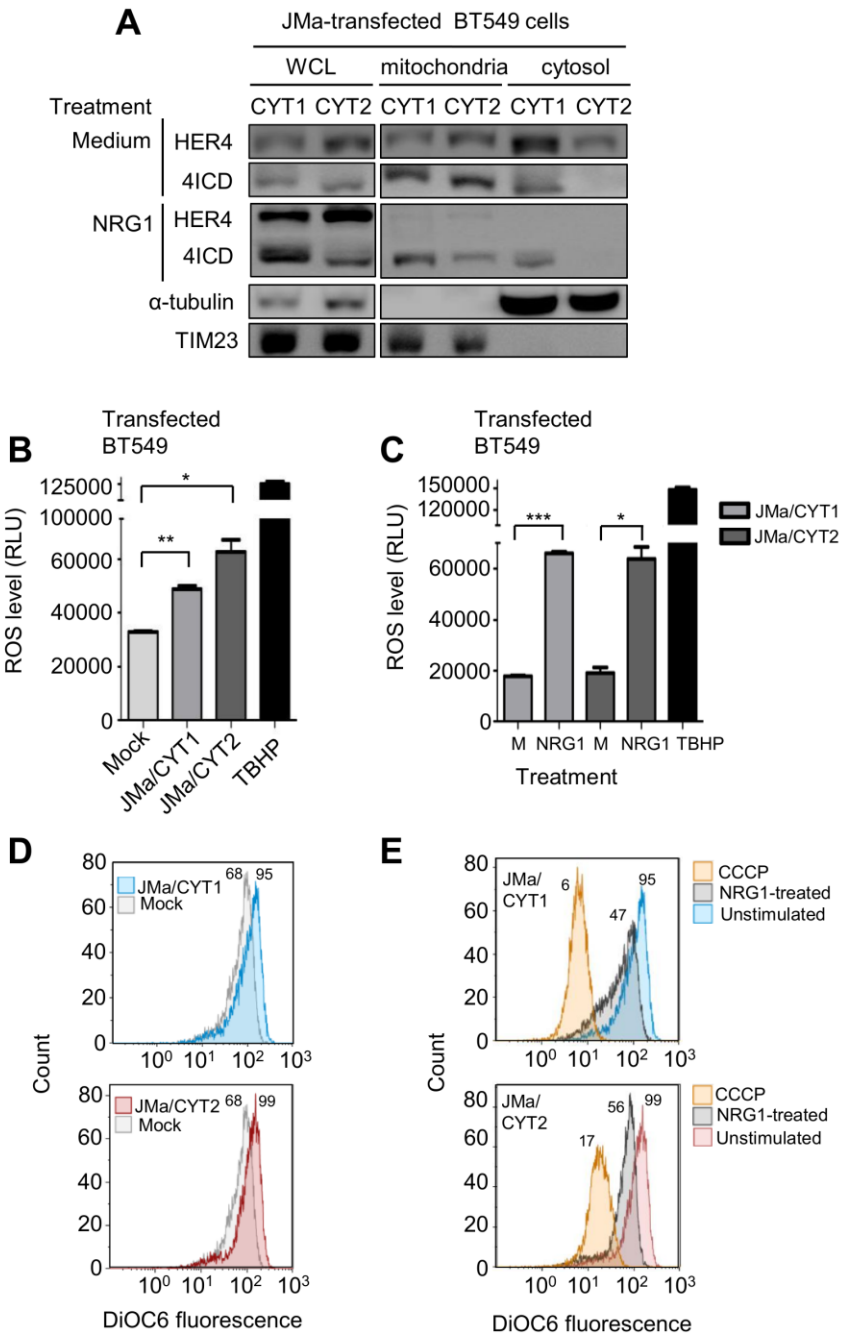
A
JMa-transfected BT549 cells
WCL
mitochondria
cytosol
Treatment
CYT1 CYT2 CYT1 CYT2 CYT1 CYT2
Medium
HER4
4ICD
NRG1
HER4
4ICD
α-tubulin
TIM23
B
Transfected BT549
ROS level (RLU)
125000
100000
60000
40000
20000
0
*
**
Mock
JMa/CYT1
JMa/CYT2
TBHP
C
Transfected BT549
ROS level (RLU)
150000
120000
60000
40000
20000
0
***
*
JMa/CYT1
JMa/CYT2
M NRG1 M NRG1 TBHP
Treatment
D
Count
JMa/CYT1
Mock
68
95
JMa/CYT2
Mock
68
99
DiOC6 fluorescence
E
Count
JMa/ CYT1
6
47
95
CCCP
NRG1-treated
Unstimulated
JMa/ CYT2
17
56
99
CCCP
NRG1-treated
Unstimulated
DiOC6 fluorescence

Figure 3

1

2

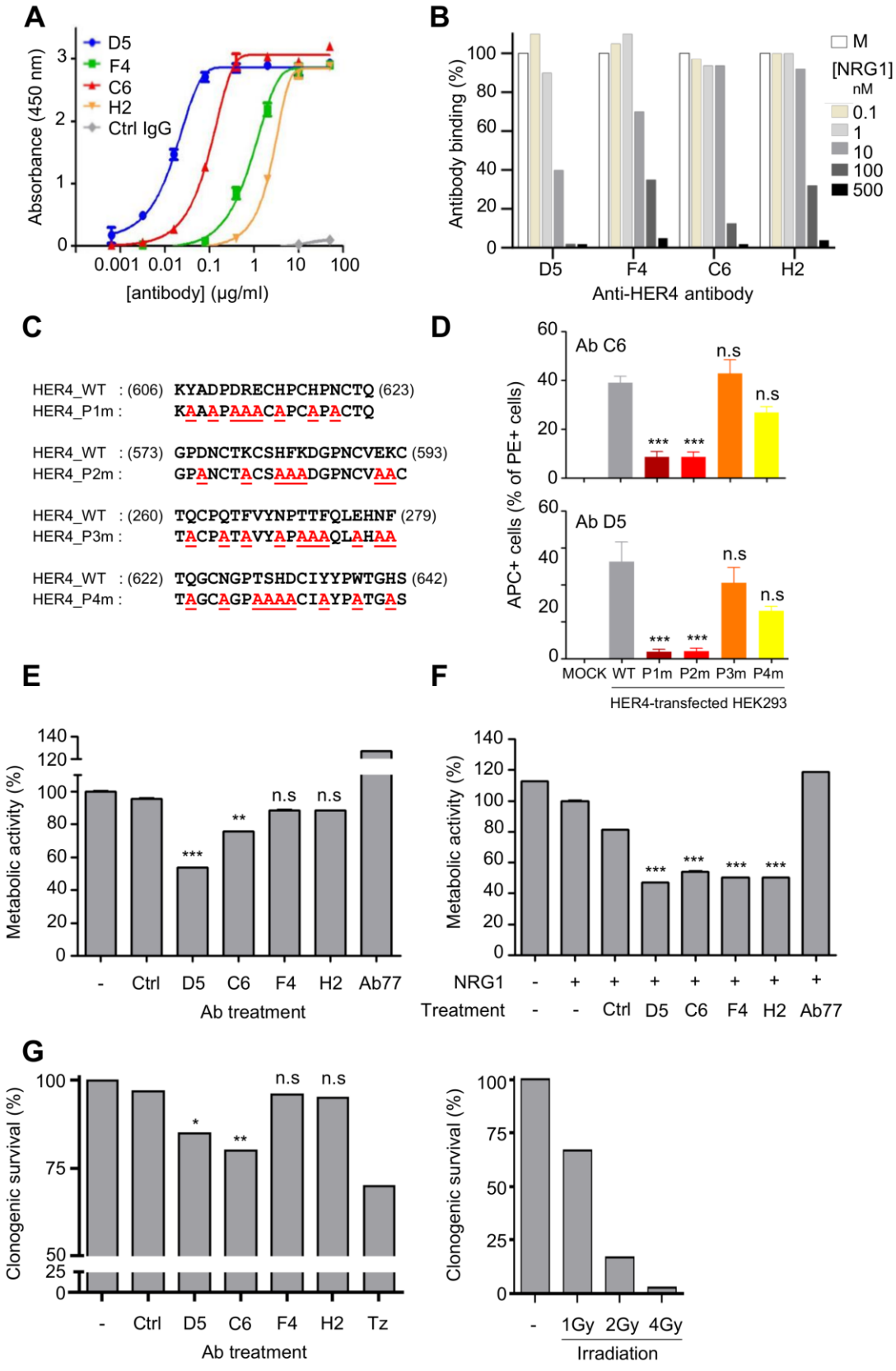
A
D5
F4
C6
H2
Ctrl IgG
Absorbance (450 nm)
[antibody] (µg/ml)
B
M
[NRG1]
nM
0.1
1
10
100
500
Antibody binding (%)
Anti-HER4 antibody
C
HER4_WT : (606) KYADPDRECHPCHPNCTQ (623)
HER4_P1m : KAAAPAAACAPCAPACTQ
HER4_WT : (573) GPDNCTKCSHFKDGPNCVEKC (593)
HER4_P2m : GPANCTACSAAADGPNCVAAC
HER4_WT : (260) TQCPQTFVYNPTTFQLEHNF (279)
HER4_P3m : TACPATAVYAPAAAQLAHAA
HER4_WT : (622) TQGCNGPTSHDCIYYPWTGHS (642)
HER4_P4m : TAGCAGPAAAACIAYPATGAS
D
Ab C6
Ab D5
APC+ cells (% of PE+ cells)
n.s
***
MOCK WT P1m P2m P3m P4m
HER4-transfected HEK293
E
Metabolic activity (%)
Ab treatment
- Ctrl D5 C6 F4 H2 Ab77
F
Metabolic activity (%)
NRG1
Treatment
- - Ctrl D5 C6 F4 H2 Ab77
G
Clonogenic survival (%)
Ab treatment
- Ctrl D5 C6 F4 H2 Tz
Irradiation
- 1Gy 2Gy 4Gy

Figure 4

1

2

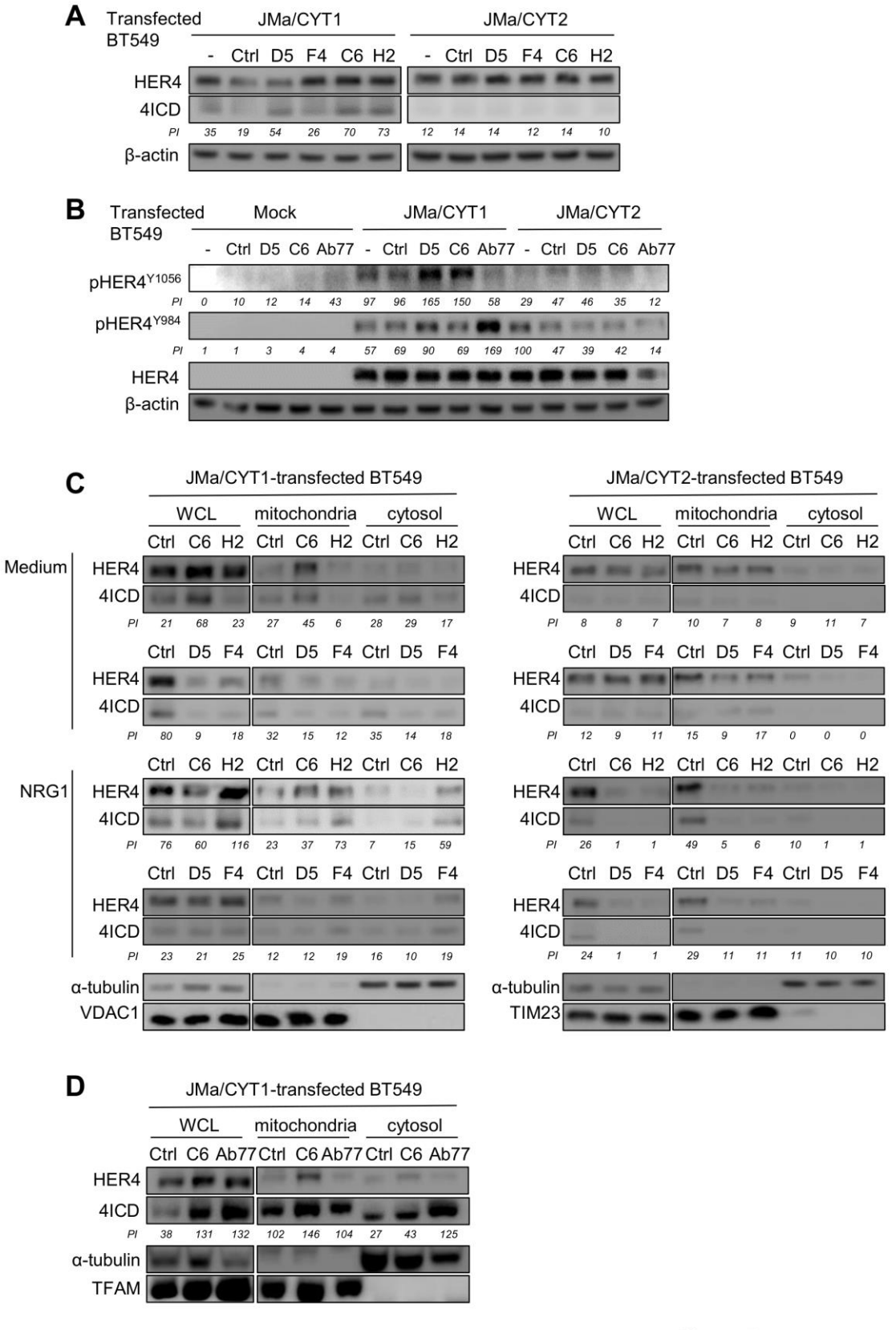
A
Transfected BT549
JMa/CYT1
JMa/CYT2
- Ctrl D5 F4 C6 H2 - Ctrl D5 F4 C6 H2
HER4
4ICD
PI 35 19 54 26 70 73 12 14 14 12 14 10
β-actin
B
Transfected BT549
Mock
JMa/CYT1
JMa/CYT2
- Ctrl D5 C6 Ab77 - Ctrl D5 C6 Ab77 - Ctrl D5 C6 Ab77
pHER4Y1056
PI 0 10 12 14 43 97 96 165 150 58 29 47 46 35 12
pHER4Y984
PI 1 1 3 4 4 57 69 90 69 169 100 47 39 42 14
HER4
β-actin
C
JMa/CYT1-transfected BT549
JMa/CYT2-transfected BT549
WCL
mitochondria
cytosol
Ctrl C6 H2 Ctrl C6 H2 Ctrl C6 H2
Medium
HER4
4ICD
PI 21 68 23 27 45 6 28 29 17
PI 8 8 7 10 7 8 9 11 7
Ctrl D5 F4 Ctrl D5 F4 Ctrl D5 F4
PI 80 9 18 32 15 12 35 14 18
PI 12 9 11 15 9 17 0 0 0
NRG1
PI 76 60 116 23 37 73 7 15 59
PI 26 1 1 49 5 6 10 1 1
PI 23 21 25 12 12 19 16 10 19
PI 24 1 1 29 11 11 11 10 10
α-tubulin
VDAC1
TIM23
D
JMa/CYT1-transfected BT549
WCL
mitochondria
cytosol
Ctrl C6 Ab77 Ctrl C6 Ab77 Ctrl C6 Ab77
HER4
4ICD
PI 38 131 132 102 146 104 27 43 125
α-tubulin
TFAM

Figure 5

1

2

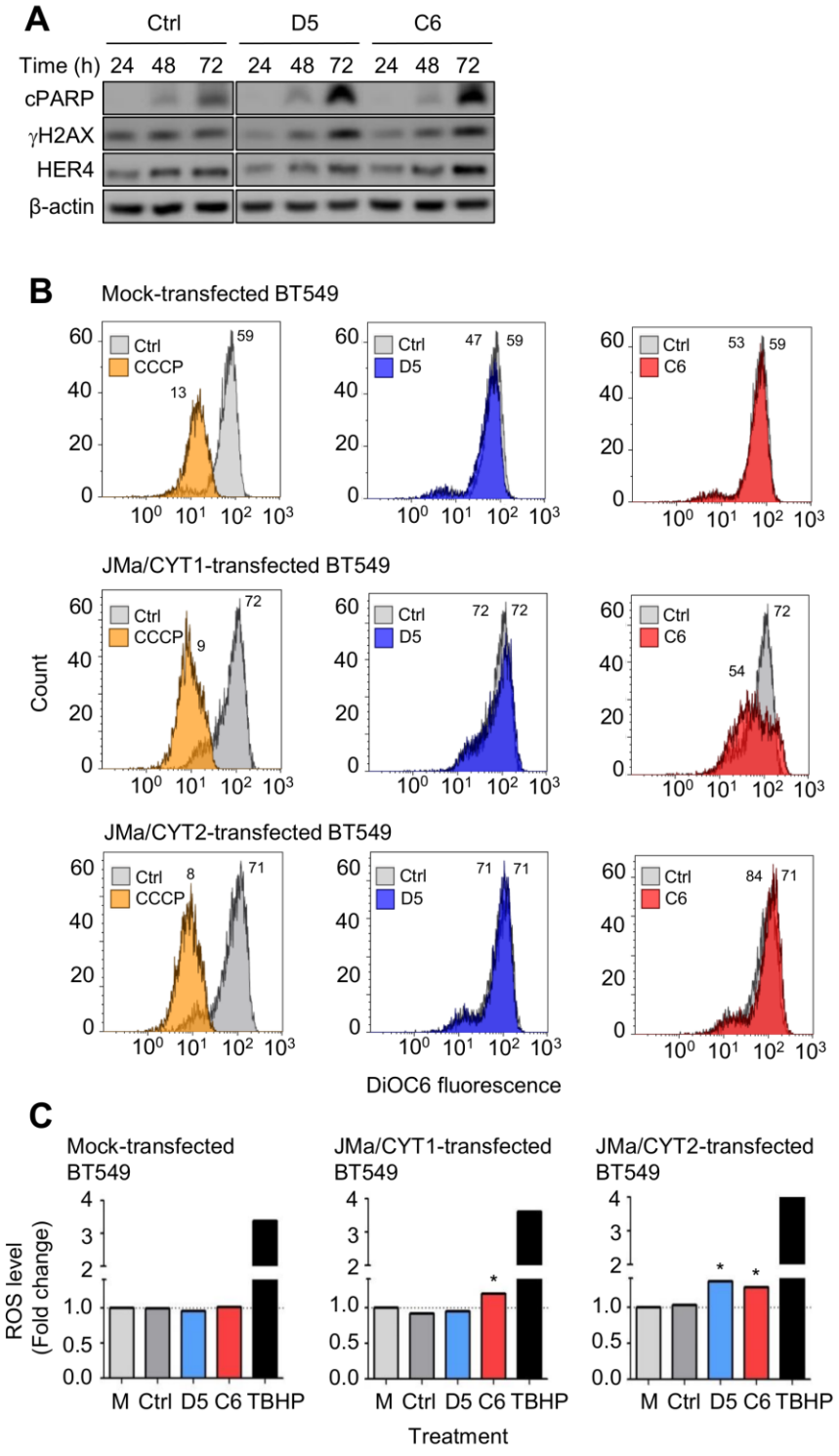
A
Ctrl
D5
C6
Time (h) 24 48 72 24 48 72 24 48 72
cPARP
γH2AX
HER4
β-actin
B
Mock-transfected BT549
JMa/CYT1-transfected BT549
JMa/CYT2-transfected BT549
Ctrl
CCCP
D5
C6
Count
DiOC6 fluorescence
C
Mock-transfected BT549
JMa/CYT1-transfected BT549
JMa/CYT2-transfected BT549
ROS level (Fold change)
M Ctrl D5 C6 TBHP
Treatment

Figure 6

1

2

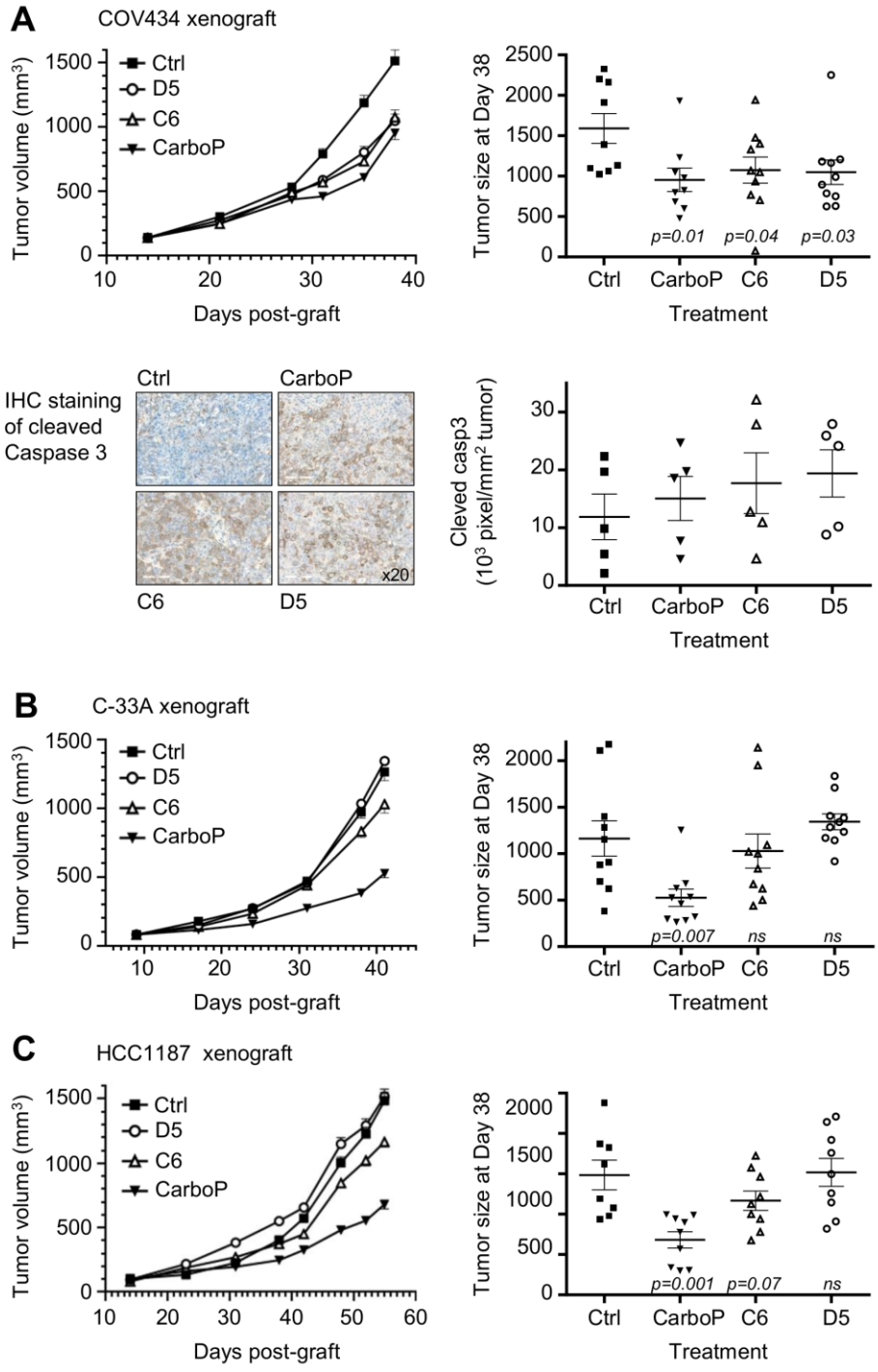
A
COV434 xenograft
Tumor volume (mm3)
Ctrl
D5
C6
CarboP
Days post-graft
Tumor size at Day 38
p=0.01
p=0.04
p=0.03
Treatment
IHC staining of cleaved Caspase 3
Ctrl
CarboP
C6
D5
x20
Cleved casp3 (10³ pixel/mm² tumor)
B
C-33A xenograft
p=0.007
ns
C
HCC1187 xenograft
p=0.001
p=0.07

Figure 7

1

2

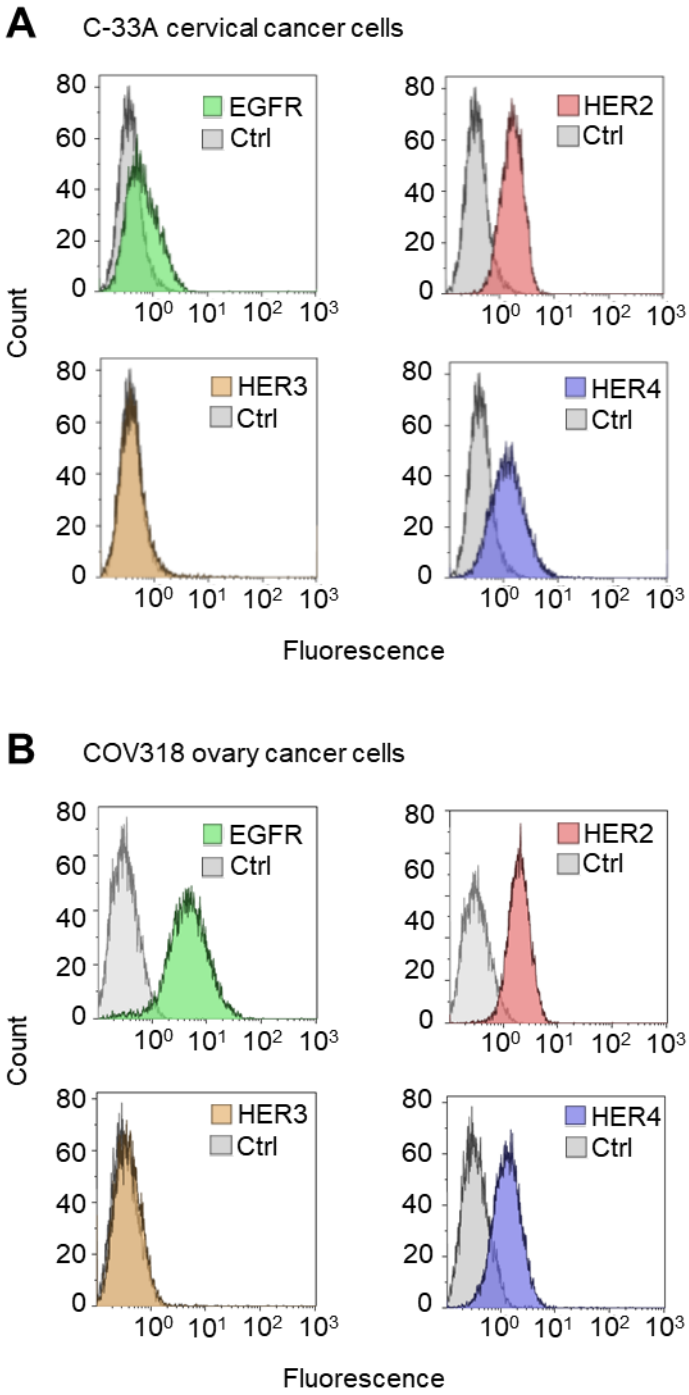

Fig.S1. Flow cytometry analysis of HER receptor expression in C-33A cervical cancer cells (**A**), and COV318 ovary cancer cells (**B**) in one experiment. Ctrl: negative control antibody.

1

2

1

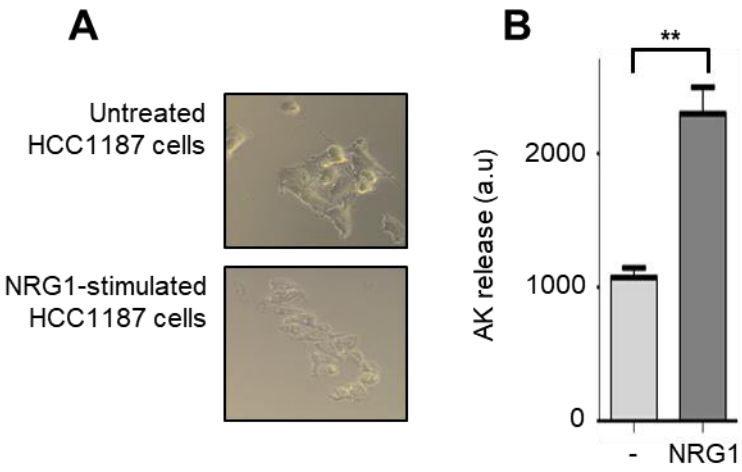

Fig. S2. (**A**) Microphotographs (microscopy magnification: x40) of unstimulated and NRG1-stimulated HCC1187 TNBC cells. Representative microphotographs are shown (n=3). (**B**) Adenylate kinase (AK) release from unstimulated and NRG1-stimulated HCC1187 cells. Cells were serum-starved for 12h, and stimulated or not with NRG1 in sextuplicate for 72h. Then, cell death was analyzed using an AK-releasing assay. Experiments were repeated two times independently and data are represented as mean ± SEM. **p<0.01 (unpaired t test).

2

3

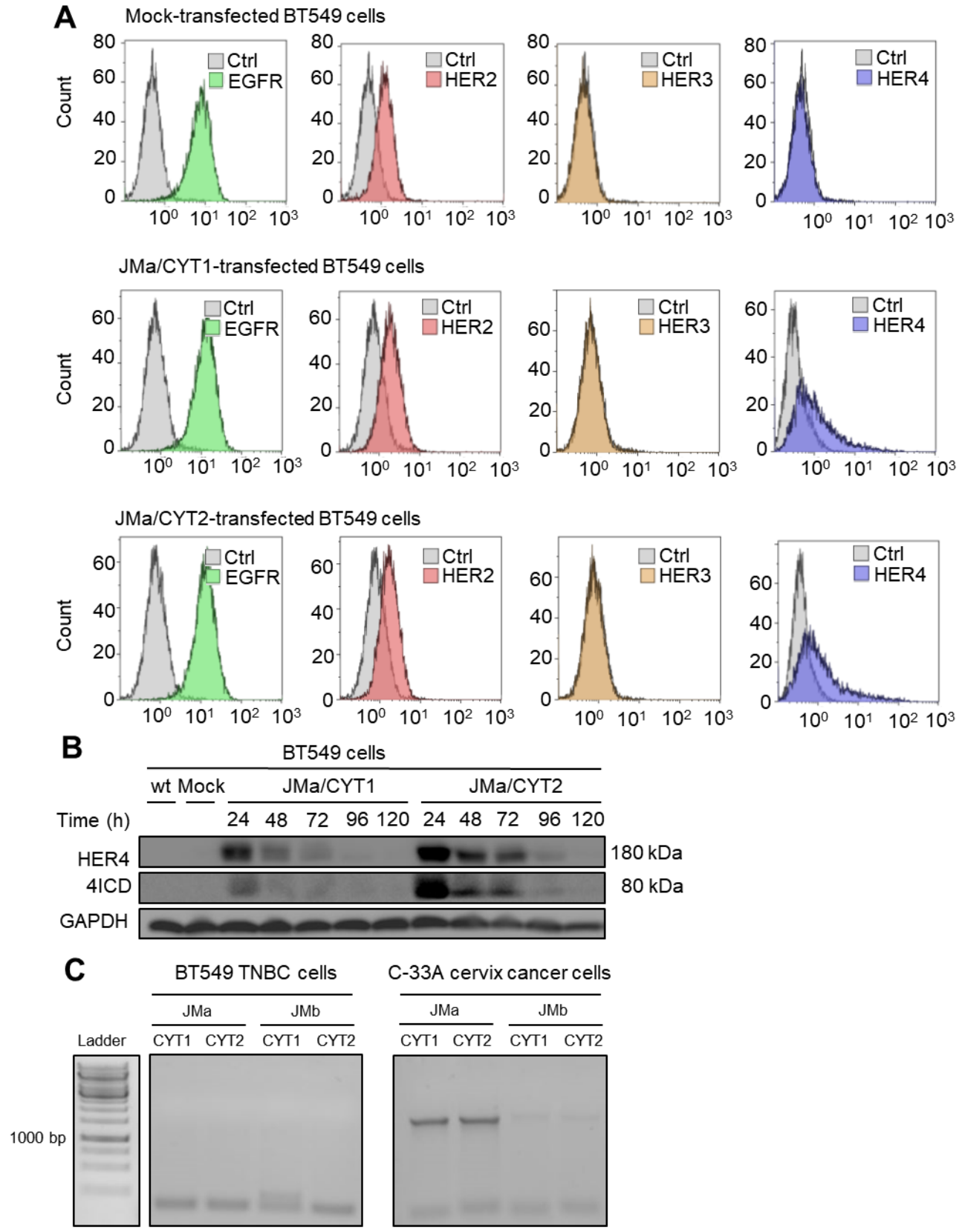

Fig. S3. (**A**) Flow cytometry analysis of HER expression in Mock-, HER4 JMa/CYT1- and JMa/CYT2-transfected BT549 cells in one experiment. Ctrl: negative control antibody. (**B**) Western blot analysis of HER4 and 4ICD expression in parental (wt), mock-, HER4 JMa/CYT1- and JMa/CYT2-transfected BT549 cells using the E200 antibody that recognizes both full-length HER4 (180 kDa) and 4ICD (80 kDa). The experiments were carried out two times and representative blots are shown. GAPDH was used as loading control. (**C**) RT-PCR analysis of HER4 isoform expression in non-transfected BT549 (TNBC) cells and C-33A (cervical cancer) cells. The experiments were performed twice.

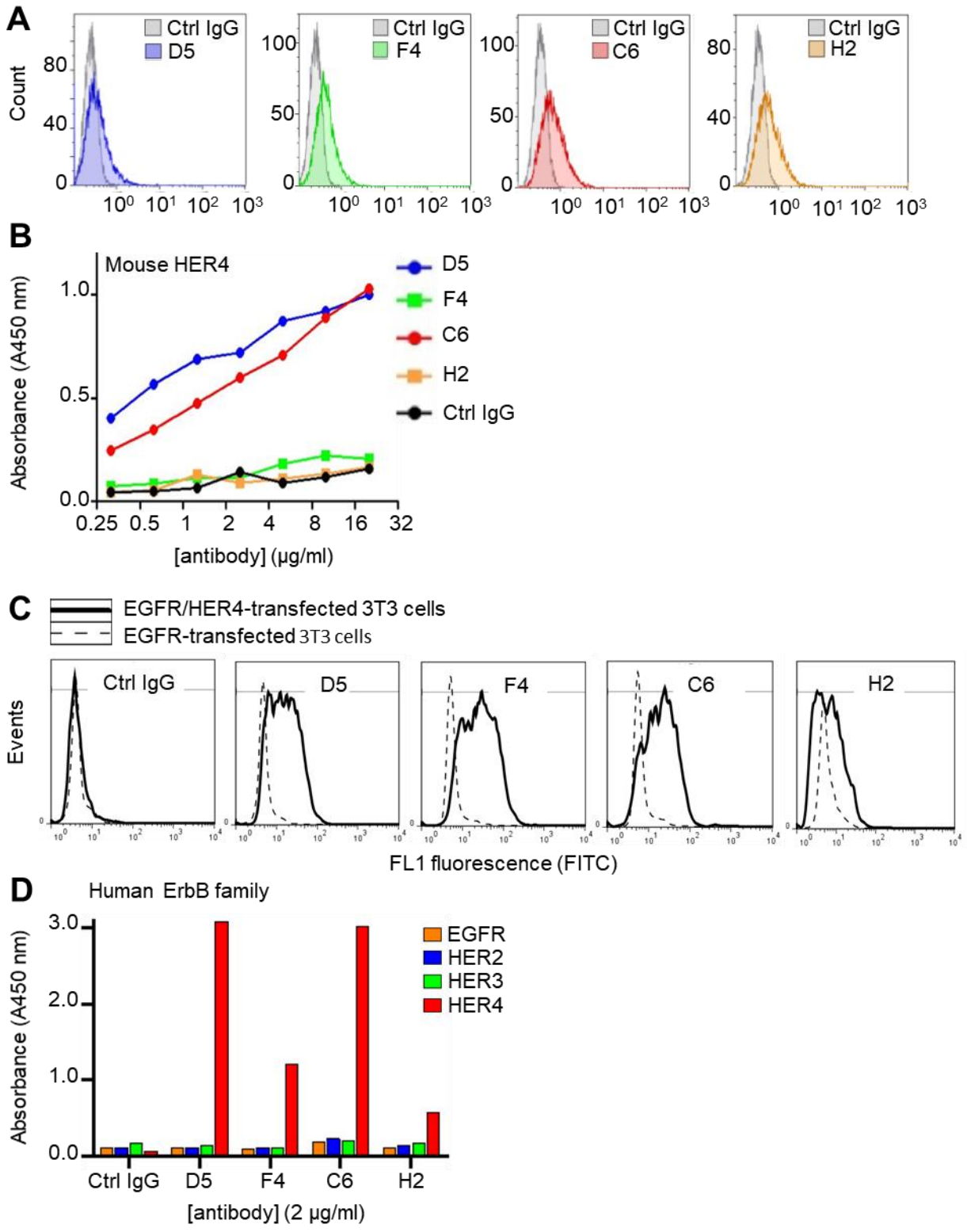

Fig.S4. (**A**) Flow cytometry analysis of the binding of the selected antibodies D5, F4, C6 and H2 in C-33A cancer cells. Analysis was carried out two times independently. Ctrl IgG: negative control antibody. (**B**) ELISA analysis of the binding of the selected anti-HER4 antibodies to mouse recombinant HER4. Ipilimumab was used as negative control antibody (Ctrl IgG). Triplicate wells were set up for each antibody dilution. (**C**) Flow cytometry binding of the selected anti-HER4 antibodies to EGFR/HER4 co-transfected vs EGFR-only transfected 3T3 cells. The experiments were repeated three times and representative cytometry profiles are shown. (**D**) ELISA binding of 2µg/ml concentration of selected anti-HER4 antibodies to ErbB family members EGFR, HER2, HER3 and HER4. Duplicate wells were set up for each antibody dilution. Ctrl IgG: negative control antibody.

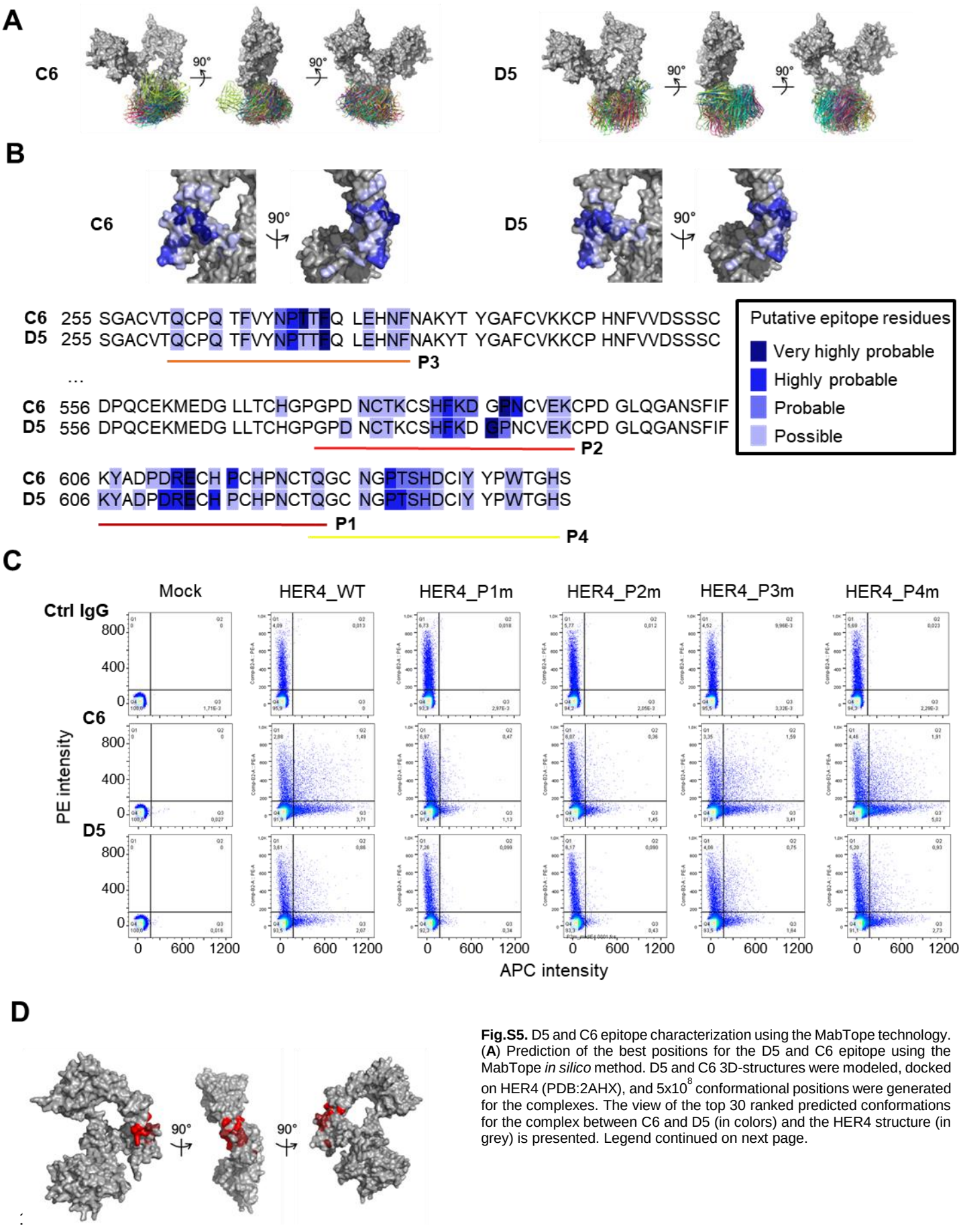

Fig.S5. D5 and C6 epitope characterization using the MabTope technology. (**A**) Prediction of the best positions for the D5 and C6 epitope using the MabTope *in silico* method. D5 and C6 3D-structures were modeled, docked on HER4 (PDB:2AHX), and $5x10^8$ conformational positions were generated for the complexes. The view of the top 30 ranked predicted conformations for the complex between C6 and D5 (in colors) and the HER4 structure (in grey) is presented. Legend continued on next page.

Fig.S5. Continued. D5 and C6 epitope characterization using the MabTope technology. (**B**) Probability for HER4 residue implication in the D5 and C6 epitopes. For each mAb, the frequency of each residue in the epitope was evaluated from the 30 best predicted interfaces. Frequency is represented in blue (darker color indicates higher probability for the residue to be implicated in the epitope). Four regions in HER4 ECD (P1 to P4) appeared to be implicated in mAb binding. (**C**) Flow cytometry analysis of C6 and D5 binding in mock-, WT HER4-, HER4 mutant (P1m-, P2m-, P3m- and P4m)-transfected HEK293 cells. Each HER4 variant harbors a mutation in one of the four predicted regions (HER4_P1m to P4m) (Figure 4C). After cell fixation, membrane HER4 expression was monitored with the PE-coupled anti-Flag antibody (ordinate), and C6 or D5 binding was measured with an APC-coupled anti-IgG antibody (abscissa). An irrelevant IgG was used as control (Ctrl). Duplicate wells were done for each condition. Data are representative of three independent experiments. (**D**) Localization of the regions 575-592 and 605-620 (involved in the conformational epitopes of anti-HER4 antibodies C6 and D5) on the HER4 crystallographic structure (PDB:2AHX).

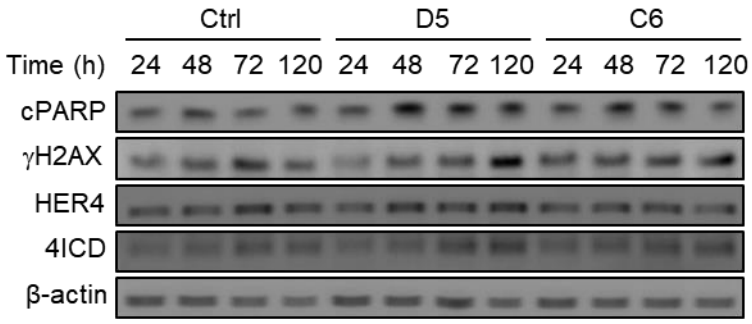

Fig.S6. Western blot analysis of COV318 cells incubated with the D5 and C6 mAbs for the indicated times. In one experiment, cleaved PARP, γH2AX, HER4 and 4ICD were detected using the appropriate primary antibodies.